







RESEARCH ARTICLE

10.1029/2024GC011516

Temperatures of Vein Formation Associated With Plate Interface Deformation Constrained by Oxygen and Clumped Isotope Thermometry

T.-W. Chen^{1,2} , A. Smye¹ , M. Lloyd¹, D. Fisher¹ , and Y. Hashimoto³ 

¹Department of Geosciences, Pennsylvania State University, University Park, PA, USA, ²Department of Earth and Space Sciences, University of Washington, Seattle, WA, USA, ³Department of Applied Science, Faculty of Science, Kochi University, Kochi, Japan

Key Points:

- Quartz-calcite veins in ancient accretionary prisms record temperatures of 100–250°C, implying a fluid-rich zone along plate interfaces
- Fluid isotopic compositions suggest rock-buffered fluids as major vein-forming fluids derived from the dehydration of host rocks
- Reduced vein formation, along with clay hydration at 250–350°C, may cause a shift in hydrogeology and mechanics of subduction fault zones

Supporting Information:

Supporting Information may be found in the online version of this article.

Correspondence to:

T.-W. Chen,
txc69@psu.edu

Citation:

Chen, T.-W., Smye, A., Lloyd, M., Fisher, D., & Hashimoto, Y. (2024). Temperatures of vein formation associated with plate interface deformation constrained by oxygen and clumped isotope thermometry. *Geochemistry, Geophysics, Geosystems*, 25, e2024GC011516. <https://doi.org/10.1029/2024GC011516>

Received 15 FEB 2024

Accepted 8 MAY 2024

Author Contributions:

Conceptualization: T.-W. Chen,

A. Smye, D. Fisher

Data curation: T.-W. Chen, M. Lloyd

Formal analysis: T.-W. Chen, M. Lloyd

Funding acquisition: A. Smye, D. Fisher

Investigation: T.-W. Chen, M. Lloyd

Methodology: T.-W. Chen, A. Smye,

M. Lloyd

Project administration: D. Fisher

Resources: T.-W. Chen, A. Smye,

M. Lloyd, Y. Hashimoto

Abstract Tectonic mélanges, characterized by conditions reflective of modern subduction fault zones, preserve mineral veins formed through mass transfer, a mechanism influencing the slip behavior of subduction megathrusts. In this study, we apply secondary ion mass spectrometry quartz-calcite oxygen isotope thermometry and clumped isotope thermometry to examine the temperatures of vein formations in six mélange units in the Cretaceous Shimanto belt and one mélange in the Kodiak accretionary prism. Calcite in the veins exhibits $\delta^{13}\text{C}_{\text{PDB}}$ values ranging from -17.2‰ to -6.8‰ , indicative of a carbon source mixing with sedimentary carbonate and organic matter. $\delta^{18}\text{O}_{\text{SMOW}}$ values of calcite range from $+11.1\text{‰}$ to $+17.2\text{‰}$; quartz yields $\delta^{18}\text{O}_{\text{SMOW}}$ values of $+14.9\text{‰}$ to $+21.7\text{‰}$. Oxygen isotopic signatures in minerals reveal that most vein-forming fluids are significantly affected by rock buffering, while some retain isotopic compositions of seawater and meteoric water. Temperature estimates, derived from both thermometers, fall within the range of 100–250°C. Notably, vein temperatures remain constant across diverse vein types and mélange units with distinct maximum temperatures. The combined temperature records and fluid isotopic compositions imply vein formations at shallower depths linked to the incorporation of seawater, meteoric water, and fluid released from early dehydration reactions. At greater depths, vein formations are associated with fluid released from clay dehydration and long-distance fluid flow. Reduced vein formations between 250 and 350°C may correlate with a shift to fluid-unsaturated conditions resulting from clay hydration reactions. Our study highlights potential mechanical and hydraulic variations within the thermal conditions of 100–350°C along the plate boundary driven by fluid-mineral interactions.

Plain Language Summary Temperature influences the processes responsible for triggering earthquakes at subduction zones. This inference is supported by the observed concentration of seismic activities within a specific temperature range along the plate interface. To investigate the topic, we examine a distinctive rock type known as tectonic mélanges, which has undergone subduction in the past and has since been exposed. These mélanges contain mineral veins formed through the movement of materials; a factor that has shown correlation with the occurrence of earthquakes at subduction zones. To determine the temperatures at which the mechanism operates, leading to the formation of the veins, we employ two methodologies: quartz-calcite oxygen isotope thermometry and clumped isotope thermometry. Our findings indicate that, regardless of the geographical locations or the types of veins, they formed within a temperature range of 100–250°C. This consistency implies the existence of a consistent depth range within subduction zones, where fluids are predominantly present, facilitating material movement and consequently, the development of these mineral veins.

1. Introduction

It has long been hypothesized that seismicity along subduction megathrusts is controlled by temperature-dependent processes. Vrolijk (1990) proposed that plate boundary décollements tend to develop in smectite-rich horizons at shallow depths, and the onset of seismic behavior may result from the transformation of smectite to illite, which occurs mostly between 100 and 150°C (e.g., Chamley, 1989; Hower et al., 1976; Jennings & Thompson, 1986). This temperature range is consistent with the modeled temperature range of the seismic fronts at several subduction zones (Hyndman et al., 1997; Oleskevich et al., 1999). However, Moore and Saffer (2001) argued that the volumetric proportion of smectite ($>\sim 30\text{--}50\%$) that would be required for this

© 2024 The Author(s). Geochemistry, Geophysics, Geosystems published by Wiley Periodicals LLC on behalf of American Geophysical Union. This is an open access article under the terms of the [Creative Commons Attribution-NonCommercial-NoDerivs License](#), which permits use and distribution in any medium, provided the original work is properly cited, the use is non-commercial and no modifications or adaptations are made.

Software: T.-W. Chen, M. Lloyd
Supervision: A. Smye, M. Lloyd, D. Fisher
Validation: T.-W. Chen, A. Smye, M. Lloyd
Visualization: T.-W. Chen
Writing – original draft: T.-W. Chen
Writing – review & editing: T.-W. Chen, A. Smye, M. Lloyd, D. Fisher, Y. Hashimoto

mineral to control plate boundary slip behavior, based on laboratory data (Logan & Rauenzahn, 1987), is too high compared to typical sediments at subduction interfaces (e.g., Hyndman et al., 1997). Illite-rich materials, despite their higher frictional strength, do not exhibit velocity-weakening behavior (Saffer & Marone, 2003), which is favored for the nucleation of an instability (e.g., Marone, 1998; Scholz, 1998). Therefore, composite changes in porosity, fluid pressure, effective stress, and rock fabrics along the plate interface due to other depth/temperature-dependent fluid production, diagenetic, and metamorphic processes such as dehydration reactions and diffusive mass transfer have been suggested to contribute to the upper aseismic-seismic transition (Moore & Saffer, 2001; Saffer & Marone, 2003).

The maximum depths of thrust-faulting earthquakes and associated temperatures, on the other hand, vary across modern convergent margins, ranging from 20 to 60 km, corresponding to 250–600°C (England & Smye, 2023). The boundaries may also differ along the same convergent margins (e.g., Li et al., 2015; Newman et al., 2002; Seno, 2005). The two leading explanations for the onset of stable creep with increasing depth along subduction interfaces are: (a) the initiation of crystalline plasticity and corresponding stable sliding behavior (e.g., Scholz, 1990) and (b) the intersection of subducting slab with the overlying forearc mantle wedge (e.g., Peacock & Hyndman, 1999). The recognition that both the updip and downdip boundaries of the seismogenic zone are related to temperature and thermally activated processes emphasizes the importance of understanding the thermal condition of subduction fault zones and the connection between temperature and hypothesized mechanisms that control plate boundary slip behavior.

Drilling to seismogenic depths at active convergent margins remains a technological challenge. However, exhumed accretionary complexes such as those exposed along the Shimanto belt in Japan and on Kodiak Island in Alaska preserve valuable records of the physical and chemical conditions relevant to the plate interface. These tectonic mélanges, which document underthrusting at temperatures broadly within the seismogenic zone, exhibit metamorphism consistent with zeolite to prehnite-pumpellyite facies (Moore et al., 1983; Sample & Moore, 1987; Taira et al., 1982; Toriumi & Teruya, 1988). Nonetheless, the absence of index minerals at these conditions makes it challenging to accurately determine the deformation-associated temperature and to discern subtle temperature variations among different units, which are required to test hypotheses regarding the specific mineralogical and rheological causes of seismicity.

To determine the thermal conditions of the mélanges, various geothermometers have been utilized as presented in Table 1 and Figure 1. Vitrinite reflectance (VR) and Raman spectra of carbonaceous material (RSCM) analyses have been employed as proxies for peak burial temperatures by examining the thermal maturity of organic matter within the mélanges (Ikesawa et al., 2005; Kiminami & Ohno, 1999; Kondo et al., 2005; Moore et al., 1983; Mukoyoshi et al., 2006; Raimbourg et al., 2017, 2019, 2021; Sakaguchi, 1996; Sample & Moore, 1987). However, because these proxies record are sensitive to the highest temperature experienced by a unit, they could be influenced by later stages of metamorphism that are not necessarily related to seismicity. For instance, in the Cretaceous Shimanto belt, the thermal structure related to the accretion of the complex was likely overprinted by the high thermal gradient resulting from the subduction of the Kula-Pacific ridge (Sakaguchi, 1996). Aside from organic indicators, illite crystallinity (IC) is an inorganic indicator of the diagenesis of clay minerals and the metamorphic grade (e.g., Frey, 1987; Kisch, 1987). Although IC is sensitive to burial temperatures, it can also be affected by other variables, including the grain size of the sample, the duration and rate of heating, the composition of host rocks, the chemical makeup of illite and/or mixed layer precursors, and the presence of organic matter (Eberl et al., 1987; Frey, 1987; Kreutzberger & Peacor, 1988; Ogunyomi et al., 1980; Yang & Hesse, 1991). Therefore, it is advised to exercise caution when using it as the sole indicator of paleotemperatures (Underwood et al., 1993).

On the other hand, mineral veins found in mélanges that result from mass transfer can offer insights into fluid-rock interactions along the plate interface by providing temperature information. Various methods have been utilized to determine these temperatures, including RSCM analyses using carbonaceous materials in the veins (Raimbourg et al., 2021) and the use of fluid inclusions (FI) trapped in the minerals (Hashimoto et al., 2012; Matsumura et al., 2003; Sakaguchi, 1996; Vrolijk et al., 1988). It is important to note that the in-situ temperature conditions at which the minerals precipitated may not coincide with the peak temperatures estimated by other geothermometers. Careful selection of veins for analysis is crucial as they can exhibit distinct textures and cross-cutting relationships that reflect different stages of deformation and varying thermal conditions along the path of underthrusting (Hashimoto et al., 2003; Yamaguchi et al., 2012).

Table 1

Summary of Previous Geothermometric Studies Conducted on Mélange Units in the Cretaceous Shimanto Belt and Kodiak Accretionary Complex

			Cretaceous Shimanto belt	
Mélange	Method	T (°C)	Source	Note
Lower Mugi ^a	RSCM ^b	163–206	Raimbourg et al. (2019)	Carbonaceous materials in matrix ^c
	VR ^d	130–150	Ikesawa et al. (2005)	Sweeney and Burnham (1990) (burial time not specified) ^e
	FI ^f	Vein I 125–195, Vein II-135–245	Matsumura et al. (2003)	Vein I-syn-mélange veins, Vein II-post-mélange veins ^g
Upper Mugi ^h	VR	170–200	Ikesawa et al. (2005)	Sweeney and Burnham (1990) (burial time not specified)
Yokonami	VR	190 (Awa), 250 (Goshikigahama)	Sakaguchi (1996)	Barker (1988)
	FI	130 (Awa), 170 (Goshikigahama)	Sakaguchi (1996)	Syn-tectonic veins (several generations of veins)
		175–225	Hashimoto et al. (2012)	Shear veins crosscutting or parallel mélange foliations
Kure	VR	220–240	Mukoyoshi et al. (2006)	Barker (1988); Sweeney and Burnham (1990) (burial time: 1 and 10 m.y.)
Okitsu	RSCM	214–252	Raimbourg et al. (2019)	Carbonaceous materials in matrix
	VR	265	Sakaguchi (1996)	Barker (1988)
	FI	210	Sakaguchi (1996)	Syn-tectonic veins (several generations of veins)
Hyuga	RSCM	207–264	Raimbourg et al. (2017)	Carbonaceous materials in matrix
		259	Raimbourg et al. (2021)	Carbonaceous materials in veins
	VR	250–270	Kondo et al. (2005)	Sweeney and Burnham (1990)
	IC ⁱ	260–300	Hara and Kimura (2008)	
	FI	250–279	Mukoyoshi et al. (2009)	
Makimine	RSCM	338	Raimbourg et al. (2021)	Carbonaceous materials in veins
		340	Kiminami and Ohno (1999)	
	VR			
			Kodiak accretionary complex	
Mélange	Method	T (°C)	Source	Note
Kodiak	RSCM	325	Raimbourg et al. (2021)	Carbonaceous materials in veins
	VR	225	Sample and Moore (1987)	Bostick et al. (1978) (burial time: 10 m.y.)
	FI	215–255	Vrolijk et al. (1988)	Syn-tectonic veins (several generations of veins)
Ghost Rocks	VR	205	Myers and Vrolijk (1986)	Syn-mélange veins
	VR	225–250	Moore et al. (1983)	Bostick et al. (1978) (burial time: 5–10 m.y.)
Uyak	FI	240–260	Vrolijk et al. (1988)	Syn-tectonic veins (several generations of veins)
	RSCM	234	Raimbourg et al. (2021)	Carbonaceous materials in veins
	FI	270–290	Vrolijk et al. (1988)	Syn-tectonic veins (several generations of veins)

^aThe lower section of the Mugi mélange. ^bRSCM—Raman spectra of carbonaceous material. ^cCarbonaceous materials for RSCM analyses were obtained either from the matrix or the veins of the mélanges. ^dVR—vitrinite reflectance. ^eVarying correlation equations for conversion from VR to maximum paleotemperature were used in each study. The equations are either time-independent or time-dependent with different assumed burial durations. ^fFI—fluid inclusion. ^gFI in veins with various textures and crosscutting relationships were used for analyses. ^hThe upper section of the Mugi mélange. ⁱIC—illite crystallinity.

In our study, we apply quartz—calcite oxygen isotope thermometry based on secondary ion mass spectrometry (SIMS) measurements and calcite clumped isotope thermometry to a diverse array of veins in the Cretaceous Shimanto belt of Japan and the Kodiak accretionary complex of Alaska. The occurrence of calcite in veins, along with the abundance of oxygen isotopes in both vein quartz and calcite, provide assessable geothermometers. The

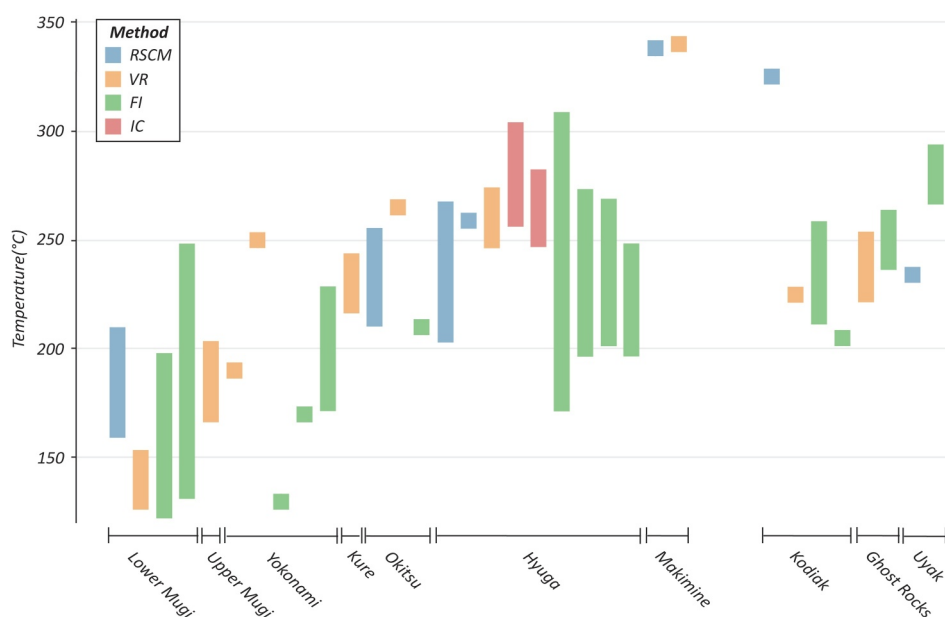


Figure 1. Compilation of published geothermometer estimates for the Cretaceous Shimanto Belt and Kodiak Accretionary Complex, with detailed data provided in Table 1. RSCM, Raman spectra of carbonaceous material; VR, vitrinite reflectance; FI, fluid inclusion; IC, illite crystallinity.

micron-scale resolution of in-situ SIMS analyses and minimal materials required for clumped isotope analyses offer the feasibility of analyzing veins with thin thickness, thereby expanding the potential to derive temperatures from veins of various generations and occurrences. Both approaches not only allow the determination of temperatures during vein mineral formation but also constrain the isotopic composition of the source fluid. By shedding light on the temperature and fluid medium associated with mass transfer, which are linked to the formation of the veins, we gain crucial insights into understanding the key components involved in seismogenesis along the plate interface.

2. Geological Setting

2.1. The Shimanto Belt

The Shimanto belt is recognized as an ancient part of the Nankai Trough accretionary prism, which is exposed on-land from the Kanto region to the Ryukyu islands in Japan. The Shimanto belt consists of Cretaceous to Miocene sediments with an overall younging trend toward the southeast. It is divided into the Cretaceous northern sub-belt and the Paleogene-Neogene southern sub-belt based on the stratigraphic age and the timing of accretion (e.g., Taira, 1980). Both sub-belts are further classified into coherent zones and mélangé zones according to the lithology and structures (Figure 2a). Coherent zones consist of alternating sandstone and mudstone beds with well-preserved sedimentary beddings. Mélangé zones are characterized by a block-in-matrix texture where blocks of sandstone are embedded in an argillaceous matrix along with slivers of basalts, tuffs, cherts, and varicolored shales showing a high degree of stratal disruption (Taira et al., 1988).

The mélangé units are sandwiched between the coherent units bounded by either paleodécollements or regional out-of-sequence thrusts, which are distinguished by the continuity or discontinuity of paleothermal structures across the faults (e.g., Hashimoto et al., 2012; Kitamura et al., 2005). Paleotemperature data also suggest that the mélangé units in the Cretaceous northern sub-belt were underthrust to temperatures characteristic of the seismogenic zone (Table 1 and Figure 1). In this study, we focus on the lower section of the Mugi mélangé (hereinafter referred to as the Lower Mugi mélangé) and Makimine mélangés, which experienced peak temperatures corresponding to the updip and downdip limits of the seismogenic zone, respectively (Table 1 and Figure 1; Ikesawa et al., 2005; Kiminami & Ohno, 1999; Matsumura et al., 2003; Raimbourg et al., 2019, 2021). We also analyze other mélangé units with intermediate temperature records including the upper section of the Mugi mélangé (hereinafter referred to as the Upper Mugi mélangé; Ikesawa et al., 2005), Yokonami (Hashimoto

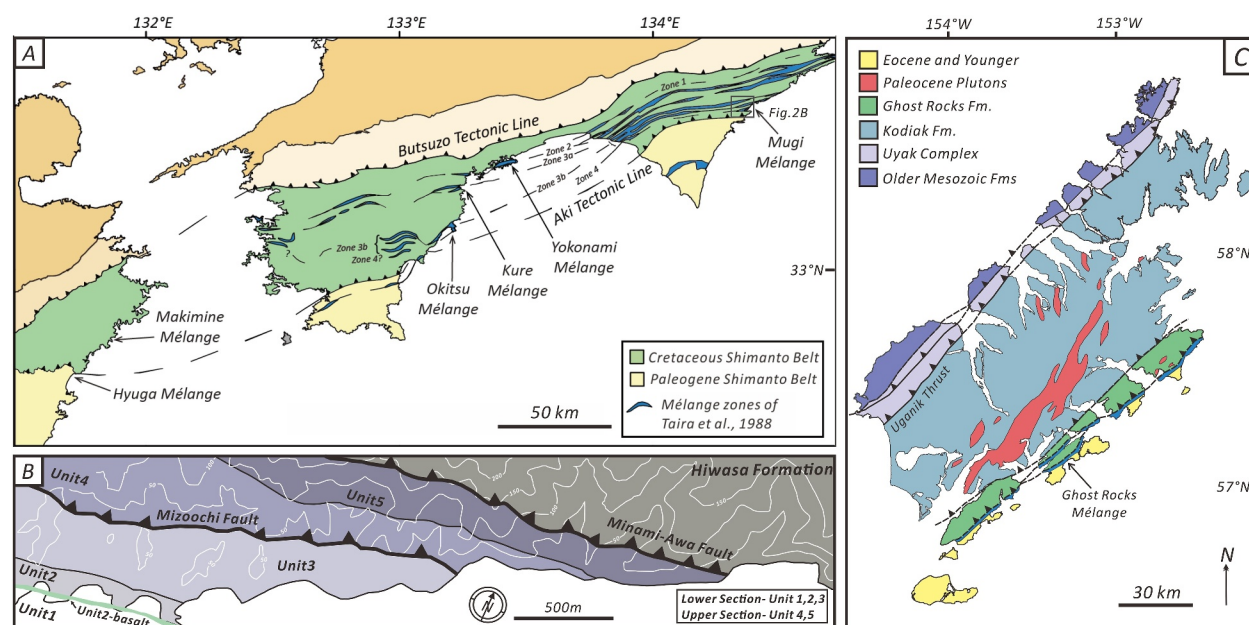


Figure 2. (a) Geological map of the Shimanto belt. The mélangé units (from Taira et al., 1988) analyzed in this study are located in the Cretaceous sub-belt. (b) Map of the Mugi mélangé (Kitamura & Kimura, 2012), which is divided into a lower and an upper section based on their paleotemperature records (Ikesawa et al., 2005). (c) Geological Map of the Kodiak accretionary complex (D. Fisher & Byrne, 1987). The Ghost Rocks mélangé is located at the southeastern side of the Ghost Rocks Formation.

et al., 2012; Sakaguchi, 1996), and Okitsu mélanges (Figures 2a and 2b; Raimbourg et al., 2019; Sakaguchi, 1996).

2.2. The Kodiak Accretionary Complex

The Kodiak accretionary complex, which shares a similar structure to the Shimanto belt, comprises a succession of accreted packages parallel to the Aleutian trench. Five accreted terraces developed in a northwestern to southeastern sequence across the complex, with a decrease in ages from late Cretaceous to Paleocene (Moore et al., 1983). This study specifically focuses on the Ghost Rocks mélangé, which is a part of the Ghost Rocks Formation. The Ghost Rocks Formation consists of coherently interbedded turbidites and stratally disrupted mélanges. The mélangé unit is situated on the southeastern side of the coherent unit and is separated from it by a paleodécollement (Figure 2c; Byrne, 1984; D. Fisher & Byrne, 1987).

2.3. Deformation in Tectonic Mélanges

The tectonic mélanges examined in this study have undergone multiple stages of deformation reflecting progressive layer-parallel shearing in concert with compaction and lithification along the plate interface. Initially, a block-in-matrix texture formed due to layer-parallel extension. The sandstone blocks within the pervasively foliated mudstone matrix exhibit boudins or pinch-and-swell structures with their long axes parallel to the foliation (Figure 3a; e.g., D. Fisher & Byrne, 1987; Kitamura & Kimura, 2012; Kimura et al., 2012). A subsequent stage of deformation produced shear bands, such as Y-P and Riedel shear structures, indicating a shear sense consistent with the relative direction of paleo-convergence. The mélangé fabrics were reoriented, with the phyllosilicates and sandstone boudins parallel to the P surface, at a low angle to Y shear surfaces. Riedel shear planes either cut through or stop at the margins of sandstone blocks (Figure 3b; e.g., Kitamura & Kimura, 2012; Kimura et al., 2012; Kondo et al., 2005).

Localized shearing of the mudstone caused an array of anastomosing microfaults to develop as it became more cohesive. Cataclastic shear occurred along with pressure solution along the microfaults, creating scaly fabrics that are characterized by polished and striated surfaces. The development of scaly microfaults was contemporaneous with tension cracking in sandstone blocks, which also experienced increased cohesion (e.g., D. Fisher & Byrne, 1987). Tensile cracks develop in the thinned areas at the margins of sandstone blocks and were

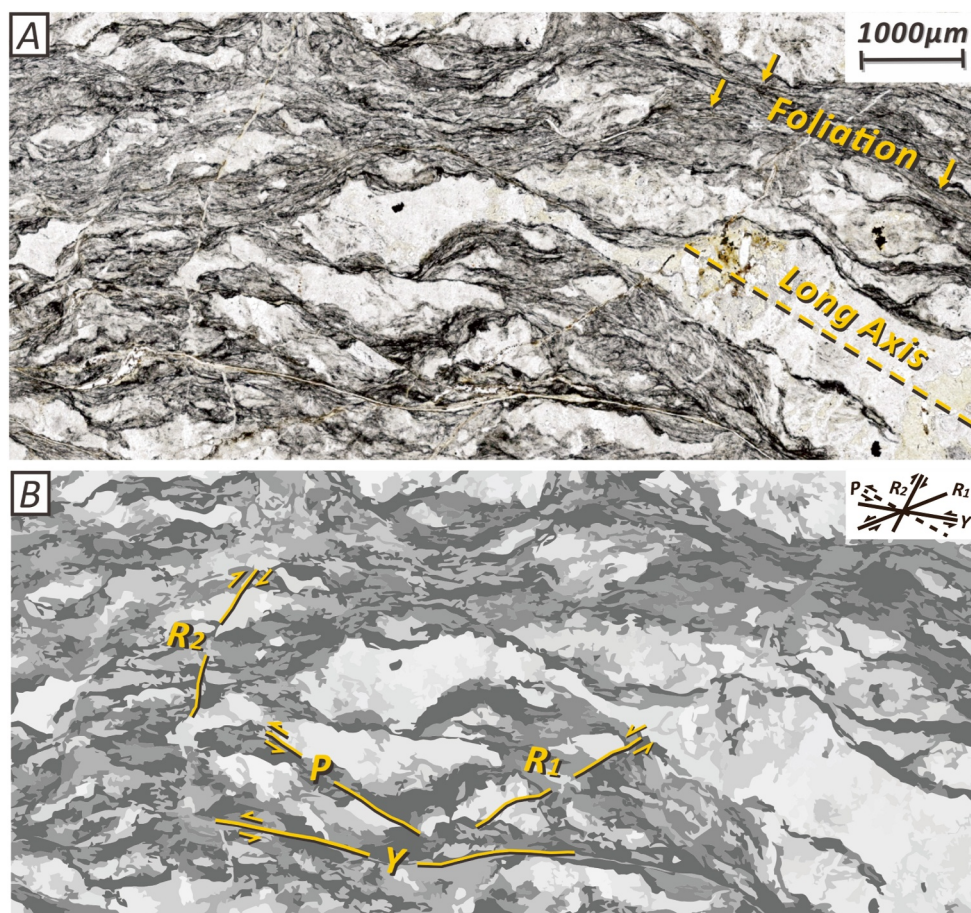


Figure 3. (a) Photomicrograph of a sample collected from the Waterfall Bay mélangé in the Kodiak Formation, which exhibits the typical block-in-matrix texture of subduction mélangés. Sandstone lenses are surrounded by the pervasively foliated mudstone matrix with their long axes parallel to the foliation. (b) Line drawing of the photomicrograph, where the YPR surfaces are annotated.

perpendicular to the long axes of the blocks and the mélangé foliation (e.g., Byrne, 1984; D. Fisher & Byrne, 1987; D. M. Fisher et al., 2019; Kimura et al., 2012; Kitamura & Kimura, 2012). Most cracks were sealed with minerals, which was likely due to local element redistribution involving dissolution along scaly fabrics, diffusion into open cracks, and crack-seal precipitation (Chen, Smye, Fisher, et al., 2024; D. M. Fisher et al., 2019; Ramirez et al., 2021). The veins are typically composed of quartz and/or calcite, with calcite grains preserved in the middle and quartz grains grown on both sides in calcite-dominated veins. These subvertical extension veins were considered as “syn-mélangé veins,” which record the pressure-temperature (P-T) conditions at which the tectonic mélangés formed along the plate interface (Hashimoto et al., 2003; Matsumura et al., 2003).

Abundant veins parallel to the foliation, previously referred as foliation-parallel veins can be observed between the sandstone blocks (e.g., Raimbourg et al., 2019; Ujiie et al., 2018). Raimbourg et al. (2019) reported that these veins preserve the crystallographic orientation and cyclic events of cracking and sealing, indicating a similar kinematic framework with the opening-mode cracking in the sandstone blocks. They could either originate from vein materials stretched off sandstone blocks (e.g., D. M. Fisher et al., 2019) or from fluid precipitation when the foliation was reactivated as microfaults (e.g., Hashimoto et al., 2012). Another set of shear veins precipitates along the shear surfaces, cutting the foliation at low angles. Slickenfibres were found on the vein surfaces (e.g., Hashimoto et al., 2012; Ujiie et al., 2018). Although it is challenging to determine the relative ages between the subvertical extension veins, foliation-parallel veins, and shear veins, the postulated relationship between the formation of foliation-parallel veins and microfaulting, and the discovery of slickenfibres on the surfaces of shear veins, both suggest their possible precipitation under a brittle regime. This implies that the formation of these

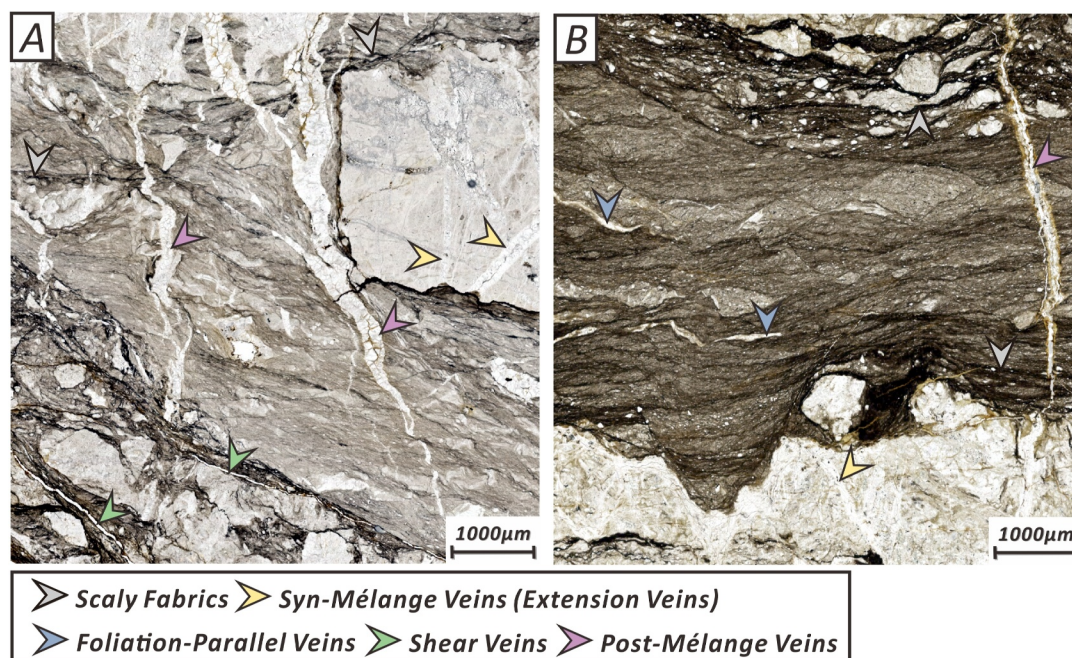


Figure 4. Photomicrographs of samples collected from the (a) Hyuga and (b) Kure mélanges of the Cretaceous Shimanto belt. The gray arrows indicate the scaly fabrics characterized by dark seams due to pressure solution. The yellow, blue, green, and purple arrows mark the extension veins restricted in the sandstone lenses, the foliation-parallel veins, the veins associated with shear surfaces, and the post-mélange veins cutting across the entire mélangé fabrics.

veins likely occurred at greater depths, when the block-in-matrix texture was established, and the sediments were more compacted and lithified.

There is another set of veins crosscutting the mélangé fabric, including both the sandstone blocks and mudstone matrix at a high angle, unlike the extension veins which are only restricted to the sandstone boudins despite their similar orientation. These veins are thought to have formed during the duplex underplating that occurred after the mélangé formation during underthrusting (e.g., Hashimoto et al., 2002). Therefore, they are classified as “post-mélange veins” in previous literature (Figure 4; Hashimoto et al., 2002; Kondo et al., 2005). Some studies that have investigated several generations of veins (e.g., Sakaguchi, 1996; Vrolijk et al., 1988), including but not limited to the above occurrences, refer them as “syn-tectonic veins” to indicate their association with multiple stages of deformation related to plate motion (e.g., Vrolijk et al., 1988).

3. Analytical Methods

3.1. Secondary Ion Mass Spectrometry

In each polished thin section of six mélangé units, one or two veins were identified using a petrographic microscope. A total of 14 veins consisting of quartz and calcite were targeted and examined (Table 2). The areas of interest were cut from the thin sections using a wire saw and embedded in epoxy resin. The mounts were then finely polished (0.25 µm) and assessed for flatness using a reflected-light microscope. In-situ isotopic measurements of both quartz and calcite (Figure 5) were performed on a Cameca 1270 Secondary Ion Mass Spectrometer (SIMS) at the University of California at Los Angeles (UCLA) SIMS Laboratory. The measurements were carried out over three analytical sessions in 2019, 2021, and 2022.

During each session, samples were sputtered with a $^{133}\text{Cs}^+$ primary beam with impact energy of 20 keV and an intensity of ~ 2 nA. The primary beam was focused to spots with a diameter in the range of 15–25 µm. The sputtered secondary ions were then accelerated into the mass spectrometer, which simultaneously measured the ion beams of oxygen isotopes $^{16}\text{O}^-$ and $^{18}\text{O}^-$ on two F cups (read through 10^{10} and 10^{11} Ω resistors, respectively) in multicollection mode. Typical intensities of $\sim 3 \times 10^9$ counts per second (cps) for $^{16}\text{O}^-$ were obtained during measurements. Each spot was analyzed for 8–10 cycles of 10 s integration, resulting in a typical internal

Table 2

List of Localities, Texture, and Nearby Maximum Temperature Records of the Analyzed Mélange Samples in This Study

Mélange	Sample #	Method	Location	Vein type	Nearby maximum temperature record				
					Method	Sample #	T (°C)	SD ^a (°C)	Reference
Cretaceous Shimanto Belt									
Lower Mugi	004,6-16	Qz-cal ^b	33.6692°, 134.4456°	Extension veins in sandstone boudins	RSCM	HN457	176	34	Raimbourg et al. (2019)
	003G-16	Clumped ^c	33.6737°, 134.4554°	Extension veins in sandstone boudins, post-mélange veins	RSCM	HN452 HN454	163 206	39 46	Raimbourg et al. (2019)
Upper Mugi	J-1 002	Qz-cal	33.6833°, 134.4769°	Extension veins in sandstone boudins	VR	In unit5	246 ^d		Ikesawa et al. (2005)
	9	Clumped	33.6843°, 134.4778°	Shear veins					
Yokonami (Awa)	8	Qz-cal	33.3713°, 133.2674°	Post-mélange veins	VR	AW1007	193 ^e		Sakaguchi (1999)
Yokonami (Goshikigahama)	14	Qz-cal	33.4247°, 133.4571°	Post-mélange veins	VR	YK1066	247		Sakaguchi (1999)
Okitsu	G17-17	Qz-cal	33.2192°, 133.2444°	Post-mélange veins	VR	KB1000	229		Sakaguchi (1999)
					RSCM	HN321	214	21	Raimbourg et al. (2019)
	3	Qz-cal	33.1804°, 133.2108°	Extension veins in sandstone boudins	VR RSCM	KB1001 HN329	234 252	9	Sakaguchi (1999) Raimbourg et al. (2019)
Makimine	027,27-16	Qz-cal	32.7281°, 131.8583°	Extension veins in sandstone boudins	RSCM	18NOB23	338	10	Raimbourg et al. (2021)
Kodiak Accretionary Complex									
Ghost Rocks	GR4-1	Clumped	57.4359°, -152.4040°	Post-mélange veins	RSCM	19KO13C	221	20	Rajič, Raimbourg, Famin, et al. (2023)
	GR7-4	Clumped	57.4342°, -152.4546°	Post-mélange veins					
	GR8-1	Qz-cal, clumped	57.4342°, -152.4552°	Post-mélange veins					

^aStandard deviation. ^bQuartz-calcite oxygen isotope thermometry. ^cClumped isotope thermometry. ^dThe R_o values reported in Ikesawa et al. (2005) and Barker's (1988) method are used to estimate maximum temperature. ^eThe R_m values reported in Sakaguchi (1999) and Barker's (1988) method are used to estimate the maximum temperature.

measurement error of <0.1‰ (1 SE). To estimate external reproducibility, each 10–20 spot analyses on samples were bracketed by 3–5 analyses of quartz and calcite standards (quartz: NL615, $\delta^{18}\text{O} = +12.33\text{‰}$, Marin et al., 2010; QzCWRU, $\delta^{18}\text{O} = +24.52\text{‰}$; UWQ-1, $\delta^{18}\text{O} = +12.33\text{‰}$, Kelly et al., 2007 calcite: Joplin calcite, $\delta^{18}\text{O} = +5.8\text{‰}$; all standards and samples reported relative to VSMOW). The standard deviation of replicate analyses of these standards varied from $\pm 0.1\text{‰}$ to $\pm 0.3\text{‰}$ (1 σ). The measured $\delta^{18}\text{O}$ values were corrected for instrumental bias using the standards.

3.2. Quartz-Calcite Oxygen Isotope Thermometry

$\delta^{18}\text{O}$ values obtained from SIMS measurements on quartz and calcite grains within mineral veins (Figure 5; Table S1) were used to calculate the temperature at which isotopic equilibrium was last achieved between the mineral pairs. The calculation was based on the following empirical relationship (Sharp & Kirschner, 1994):

$$1,000 \ln \alpha = \frac{0.87(\pm 0.06) \times 10^6}{T^2}, \text{ where } \alpha = \left(\frac{1,000 + \delta^{18}\text{O}_{\text{Qz}}}{1,000 + \delta^{18}\text{O}_{\text{Cc}}} \right)$$

Measurement errors were propagated through the temperature calibration using a series of Monte Carlo simulations.

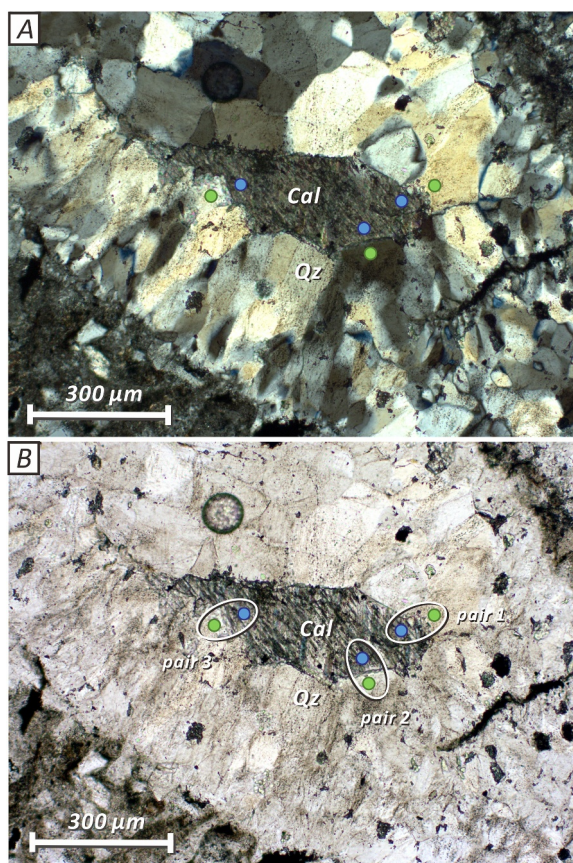


Figure 5. (a) Cross-polarized and (b) plain-polarized photomicrographs of the analyzed mineral vein in the Makimine mélange. Blue and green circles indicate point measurements conducted on calcite and quartz, respectively. Each pair of measurements allows for the calculation of the temperature associated with the mineral precipitation.

3.3. Carbonate Clumped Isotope Thermometry

Carbonate samples were collected from 11 mineral veins found in three mélange units using a Dremel microdrill (Table S2). These powders were digested, purified, and analyzed following established methods described elsewhere (Leapaldt, 2022) and summarized here. Briefly, for each sample, 8–24 mg of bulk powder (depending on the carbonate content) was reacted in a common acid bath with 104% orthophosphoric acid ($\rho > 1.92 \text{ g/cc}$) at 90°C for 20 min. Evolved CO_2 was continuously frozen in liquid N_2 over the course of the reaction. This gas was then purified using cryogenic and gas-chromatographic separations in a Protium Isotopologue Batch Extraction system (IBEX), and then introduced into the sample bellows of a Thermo MAT 253 Plus dual-inlet isotope ratio mass spectrometer. Each sample gas was analyzed relative to a working reference gas standard for 8–13 acquisitions, each of which consisted of 10 sample-standard cycles each of 26 s integration time. Most drill holes only produced enough powder to be analyzed once.

Carbonate isotopic clumping is quantified as Δ_{47} , which is defined as follows:

$$\Delta_{47} = \left(\frac{R_{47}}{R_{47}^*} - 1 \right) \times 1,000,$$

where R_{47} is the measured abundance of mass 47 isotopologues relative to mass 44 in CO_2 , and R_{47}^* is the expected abundance ratio for a stochastic (random) distribution of isotopes among all isotopologues (Ghosh et al., 2006). For each cycle, raw δ^{45} , δ^{46} , and δ^{47} values were corrected to $\delta^{13}\text{C}$, $\delta^{18}\text{O}$, and Δ_{47} values using the Brand et al. (2010) parameters as described in Daëron et al. (2016). These “raw” Δ_{47} values were projected to the carbon dioxide equilibrium scale using carbonate standards ETH1-3 (Bernasconi et al., 2021). Sample $\delta^{13}\text{C}$ and $\delta^{18}\text{O}$ values were corrected to international reference frames using the same standards. Δ_{47} values were converted to temperatures using the calcite calibration of Anderson et al. (2021), (Table S2). Measurement errors were propagated through the temperature conversion using a series of Monte Carlo simulations.

4. Results

4.1. Carbon and Oxygen Isotopic Signatures

The isotopic results are summarized in Figure 6, Table S1 and S2 (Chen, Smye, Lloyd, et al., 2024). Generally, the $\delta^{18}\text{O}$ values of quartz veins from the mélange units of the Cretaceous Shimanto belt range from $+18.0\text{‰}$ to $+21.7\text{‰}$. In contrast, the quartz in veins of the Ghost Rocks mélange in the Kodiak accretionary prism exhibit lower $\delta^{18}\text{O}$ values, ranging from $+14.9\text{‰}$ to $+15.3\text{‰}$, compared to the values observed in the mélange units of the Cretaceous Shimanto belt.

Regarding calcite, the $\delta^{18}\text{O}$ values were determined using both clumped isotope analyses and SIMS measurements. In the mélange units of the Cretaceous Shimanto belt, the $\delta^{18}\text{O}$ values of calcite in veins range from $+12.9\text{‰}$ to $+17.2\text{‰}$. Conversely, the veins in the Ghost Rocks mélange show lower $\delta^{18}\text{O}$ values, ranging from $+11.1\text{‰}$ to $+11.6\text{‰}$ based on SIMS measurement. Clumped isotope analysis of the same type of veins in the Ghost Rocks mélange yield values ranging from $+13.2\text{‰}$ to $+15.4\text{‰}$.

Furthermore, the $\delta^{13}\text{C}$ values of calcite in veins from the mélanges of the Cretaceous Shimanto belt range from -17.2‰ to -12.0‰ , while the Ghost Rocks mélange exhibits distinct values of -8.0‰ and -6.8‰ in one sample, with the other two samples showing values similar to the veins in the Cretaceous Shimanto belt, ranging from -13.5‰ to -12.5‰ .

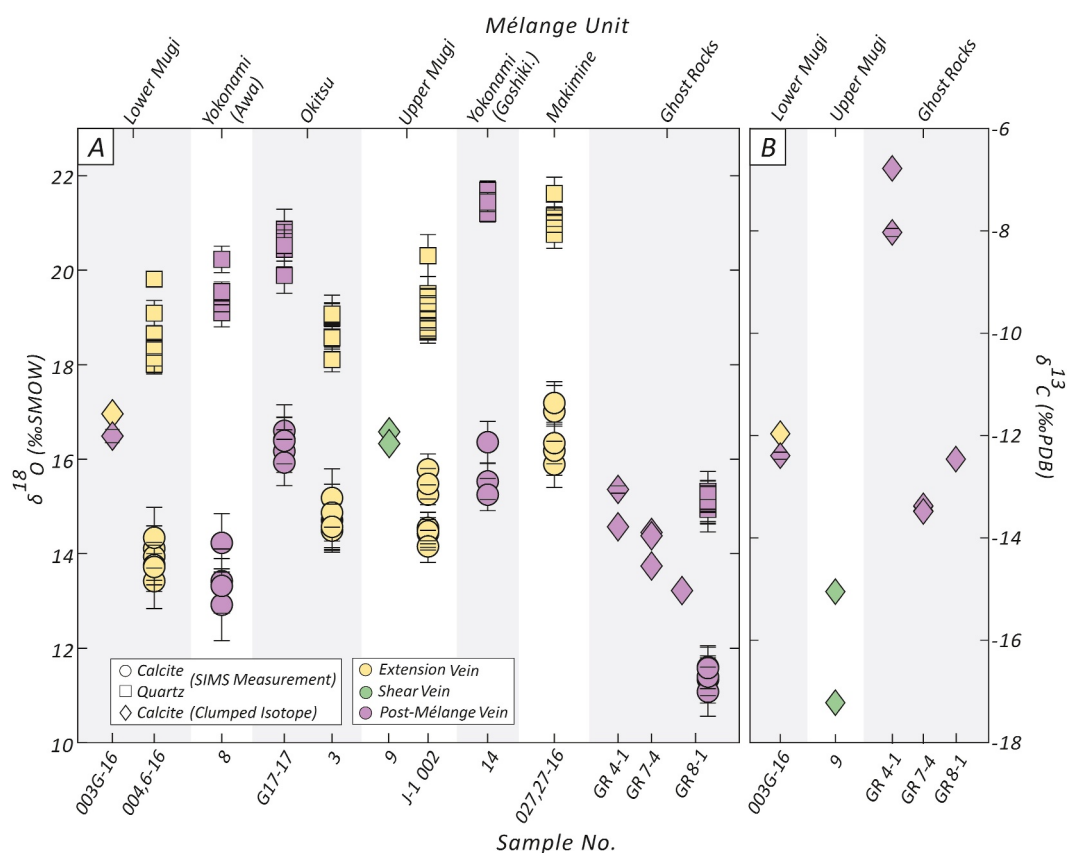


Figure 6. (a) O-isotopic compositions of quartz and calcite and (b) C-isotopic composition of calcite within veins found in tectonic mélanges of the Cretaceous Shimanto belt and Kodiak accretionary complex. $\delta^{18}\text{O}$ values of calcite and quartz are obtained using the secondary ion mass spectrometry measurement (represented by circles and squares) and clumped isotope analysis (diamonds). $\delta^{13}\text{C}$ values of calcite are determined solely through clumped isotope analysis (diamond). Colors assigned to the symbols correspond to different types of veins.

4.2. Temperature Estimates

The corresponding temperature estimates obtained from the analyses are presented in Figure 7, Table S1 and S2. For the mélanges units in the Cretaceous Shimanto belt, temperatures calculated using pairs of quartz-calcite oxygen isotope values fall within the range of 75–231°C. Results derived from clumped isotope analysis range from 134 to 182°C. Notably, there is no discernible trend between the occurrence of veins and the temperatures they record. Different types of veins within the same mélanges units exhibit similar temperature ranges. For instance, both extension and post-mélange veins in the Lower Mugi and Okitsu mélanges, as well as extension and shear veins in the Upper Mugi mélanges, share comparable temperature ranges. Temperature estimates for veins within the Ghost Rocks mélanges are 200–231 and 175–257°C using quartz-calcite oxygen thermometry and clumped isotope thermometry respectively. While there are some slightly higher temperature records, the majority of the results align with the temperature range observed in veins within the Cretaceous Shimanto belt.

5. Discussion

5.1. Fluid Sources Associated With Vein Precipitation

5.1.1. Cretaceous Shimanto Belt

The $\delta^{13}\text{C}$ values of vein calcite from the Cretaceous Shimanto belt range from -17.2‰ to -12.0‰ . This range aligns with the findings of Yamaguchi et al. (2012), who report a range of -17.2‰ to -7.4‰ for the extension and post-mélange veins (referred to as boudin neck and network veins in their study) in the Lower Mugi mélanges. The similarity in results suggests a comparable carbon source for our vein samples, which is a mixture of organic

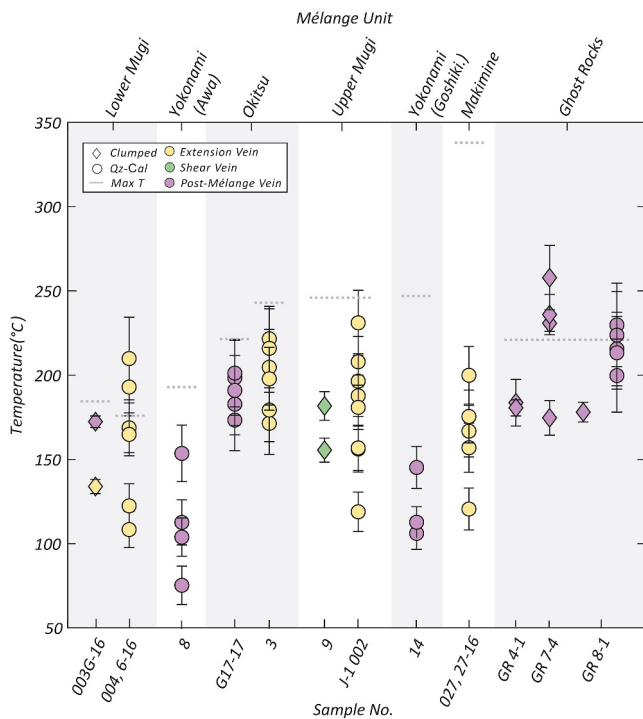


Figure 7. Temperature records derived from mineral veins in the tectonic mélanges using quartz-calcite oxygen isotope thermometry and carbonate clumped isotope thermometry. Gray dashed lines indicate the maximum temperature records in proximity to the locations of the vein samples (Table 2).

matter (-25.0‰) and sedimentary carbonate (0‰). Our $\delta^{18}\text{O}$ values of calcite ($+12.9\text{‰}$ to $+17.2\text{‰}$) are lower than the range estimated by Yamaguchi et al. (2012; $+16.0\text{‰}$ to $+18.7\text{‰}$) for the extension and post-mélange veins. The $\delta^{18}\text{O}$ values of vein quartz ($+18.0\text{‰}$ to $+21.7\text{‰}$) are consistent with the estimates from Raimbourg et al. (2015; $+17\text{‰}$ to $+21\text{‰}$) for the Hyuga mélange in the Shimanto belt.

Combining the $\delta^{18}\text{O}$ values of calcite with temperature estimates derived from each method, we can determine the oxygen isotopic compositions of the vein-forming fluids ($\delta^{18}\text{O}_{\text{fluid}}$) using the empirical equation (O'Neil et al., 1969) under the assumption of isotopic equilibrium:

$$1,000 \ln \alpha = \frac{2.78 \times 10^6}{T^2} - 3.39, \alpha = \frac{\delta^{18}\text{O}_{\text{CaCO}_3}}{\delta^{18}\text{O}_{\text{fluid}}}$$

The estimated $\delta^{18}\text{O}_{\text{fluid}}$ values range from -6.7‰ to $+8.1\text{‰}$ (Figure 8, Table S1 and S2), similar to the range suggested by previous studies on veins in the Cretaceous Shimanto belt ($+1.8\text{‰}$ to $+8.7\text{‰}$, Yamaguchi et al., 2012) and Franciscan Complex (-3‰ to $+14\text{‰}$, Sadofsky & Bebout, 2001).

Raimbourg et al. (2015) identified two distinct types of quartz in mineral veins within the Hyuga mélange of the Cretaceous Shimanto belt using quartz cathodoluminescence (CL). These quartz types are linked to different fluid sources: one associated with bound water, released locally from hydrous minerals through dehydration reactions, and the other connected to seawater that percolates externally downward due to post-seismic flow. The distinction between the quartz types is based on the unique salinity and aluminum signatures preserved within each type. The findings parallel with the interpretation proposed by Yamaguchi et al. (2012) regarding the fluids responsible

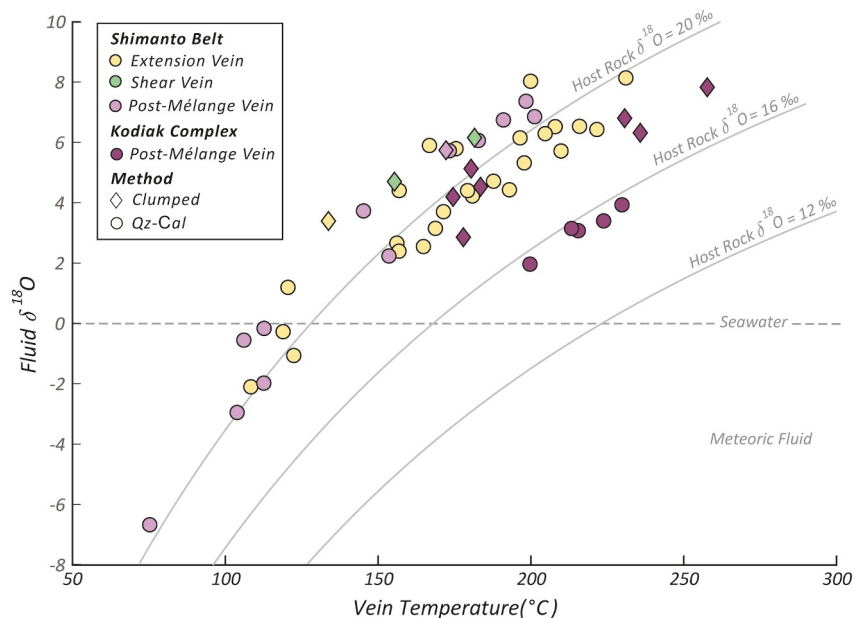


Figure 8. Plot of O-isotopic compositions of vein-forming fluids versus vein temperatures. The curves depict fluid isotopic compositions when in equilibrium with quartz with $\delta^{18}\text{O}$ values of 12‰ , 16‰ , and 20‰ . The dashed line indicates the isotopic composition of seawater ($\delta^{18}\text{O} = 0$), with the area below representing the range for meteoric water ($\delta^{18}\text{O} < 0$). Circles and diamonds represent data obtained from quartz-calcite oxygen isotope and clumped isotope thermometry, respectively. The colors assigned to the symbols correspond to different types of veins.

for vein formation in the Lower Mugi mélange. They suggest that the vein-forming fluids in the mélange comprise a mixture of seawater and rock-buffered fluids, as indicated by the strontium and oxygen isotopic compositions of the vein materials. Rock-buffered fluid sources likely originate from the dehydration reactions such as smectite-illite transition and saponite-chlorite transition occurring in subducted terrigenous sediments and oceanic crust, respectively (Kameda et al., 2011; Merriman & Frey, 1999; Moore & Saffer, 2001; Vrolijk, 1990).

We compare the oxygen isotopic composition of the vein-forming fluids derived above and corresponding vein temperatures with the expected isotopic trends for three end members of potential fluids sources: meteoric water ($\delta^{18}\text{O} < 0\text{‰}$), seawater ($\delta^{18}\text{O} = 0\text{‰}$), and rock-buffered fluid. The $\delta^{18}\text{O}$ values of rock-buffered fluids are calculated under the assumption that fluids were in equilibrium with clastic quartz, with $\delta^{18}\text{O}$ values of +12‰, +16‰, and +20‰, in host rocks based on the empirical relationship for quartz-water fractionation (Sharp & Kirschner, 1994). Our findings indicate that most veins, particularly those with temperature records exceeding $\sim 130^\circ\text{C}$, predominantly formed in association with rock-buffered fluids. For extension veins with $\delta^{18}\text{O} \leq 0\text{‰}$, occurring at shallower depths along plate interfaces based on their occurrence, the oxygen signatures are likely related to seawater trapped in pore spaces of subducted sediments, and/or fluids released during early dehydration reactions. Conversely, post-mélange veins with $\delta^{18}\text{O} \leq 0\text{‰}$, being texturally later-stage, are unlikely to have precipitated at shallower depths during the early subduction path. Their occurrence and preserved low-temperature records suggest formation during exhumation. The oxygen isotopic composition reflects seawater and/or meteoric fluids surrounding the gradually uplifted mélanges due to continuous underplating, forming parts of vein-forming fluid sources. Despite the potential involvement of seawater and meteoric fluids at shallower depths, our data set aligns with the general trend of rock-buffered fluid isotopic composition, highlighting the substantial influence of host rocks on vein-forming fluids. This observation is consistent with previous studies on veins in the Cretaceous Shimanto belt (Raimbourg et al., 2015; Yamaguchi et al., 2012), Kodiak accretionary complex (Brantley et al., 1997), Franciscan Complex (Sadofsky & Bebout, 2001), and Central-Northern Apennines (Cerchiari et al., 2020; Meneghini et al., 2009; Smeraglia et al., 2020).

5.1.2. Kodiak Accretionary Complex

The $\delta^{13}\text{C}$ values of vein calcite from the Ghost Rocks mélange of the Kodiak accretionary complex exhibit a generally higher range of -13.5‰ to -6.8‰ compared to those from the Cretaceous Shimanto belt, yet they suggest a similar carbon source. The $\delta^{18}\text{O}$ values for vein calcite in the Kodiak accretionary prism ($+11.1\text{‰}$ to $+15.4\text{‰}$) are relatively low compared to those in the Shimanto belt. Similarly, our measurements for vein quartz from the Kodiak accretionary prism are comparatively lower ($+14.9\text{‰}$ to $+15.3\text{‰}$). The estimated $\delta^{18}\text{O}_{\text{fluid}}$ values for the Kodiak accretionary prism range from $+2.0\text{‰}$ to $+7.8\text{‰}$ (Figure 8, Table S1 and S2), indicating a strong influence of host rocks in vein-forming fluid, akin to the observation in the Cretaceous Shimanto belt.

However, observable offsets in vein and fluid isotopic compositions between the Kodiak accretionary prism and the Cretaceous Shimanto belt (Figures 6 and 8) suggest a divergence in the oxygen isotopic compositions of the host rocks. While the lithology of these mélanges has been simplified in the rock-buffered fluid model to sandstone predominantly composed of quartz, the actual lithology and mineralogy of host rocks are more complex. Besides sandstones, the mélanges consist mainly of mudstone matrix. In the Shimanto belt, the mudstone matrix exhibits $\delta^{18}\text{O}$ values of $+14.0\text{‰}$ to $+18.5\text{‰}$ (Masuda et al., 1992), while the mudstone matrix of the Kodiak Formation, another accreted terrace within the Kodiak accretionary complex, shows $\delta^{18}\text{O}$ values ranging from $+12.6\text{‰}$ to $+14.5\text{‰}$ (Brantley et al., 1997). A paleomagnetic investigation of the Ghost Rocks Formation suggests its formation at a latitude of $\sim 41^\circ\text{N}$ during Paleocene (Gallen, 2008). Considering that both complexes incorporate terrigenous and pelagic sediments (e.g., Taira, 1980; Yamaguchi et al., 2014), the lower $\delta^{18}\text{O}$ values in the mudstone matrix may result from the interaction of terrigenous sediments with paleo-meteoric water at higher latitude, possessing lower $\delta^{18}\text{O}$ values (e.g., Dansgaard, 1964). Consequently, the distinct oxygen isotope signatures observed in veins of these two exhumed accretionary complexes likely reflect their paleogeographic locations.

5.2. Fluid Evolution and Vein Precipitation Along the Plate Interface

Here, we integrate peak temperature records from the host rocks near our vein samples, sourced from previous studies using RSCM and/or VR (Table 2), with the vein temperatures we obtained to interpret fluid evolution and the process of vein formation along the plate interface (Figure 9). Notably, most veins formed before the mélanges

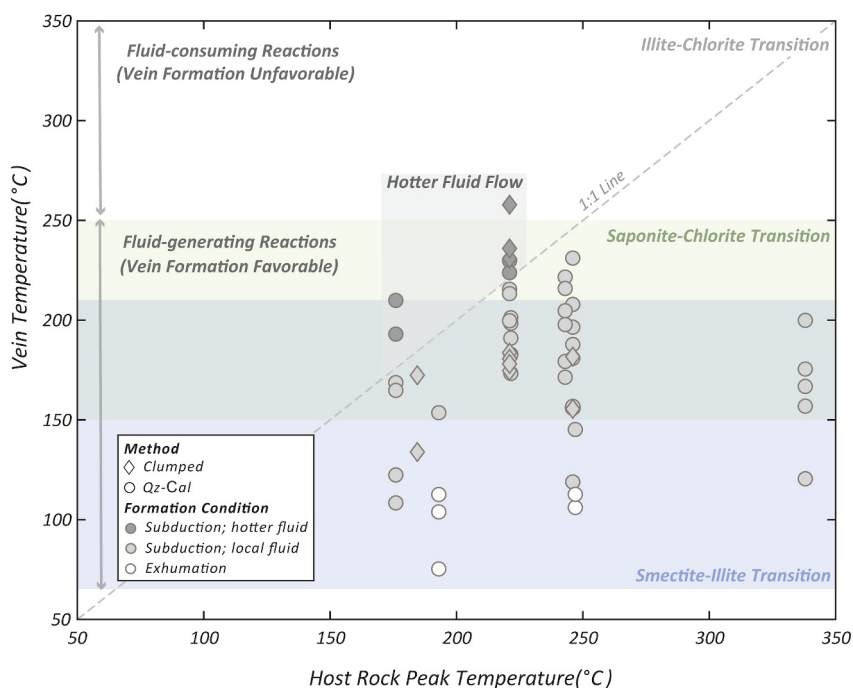


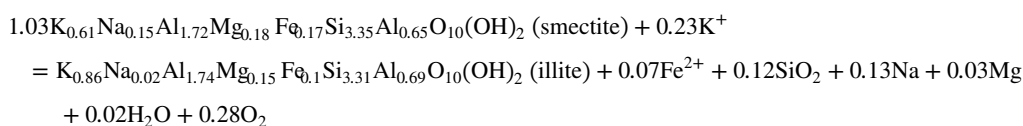
Figure 9. Plot of vein temperatures versus corresponding peak temperature recorded in country rocks. Blue and green shaded regions mark temperature ranges associated with smectite-illite and saponite-chlorite transitions, respectively, with their overlapping area shown as the dark green area. The convergence of two fluid-generating reactions establishes vein-formation favorable conditions along the plate interface. Beyond the colored regions, fluid-consuming reactions, predominantly the illite-chlorite transition, become dominant, leading to a vein-formation unfavorable condition. The gray dashed line represents the conditions where vein temperatures align with host rock peak temperatures, suggesting vein formation at maximum burial depths. Dark gray symbols above this line indicate the presence of hotter vein-forming fluids. Light gray symbols represent veins formed during the subduction path and before reaching maximum burial depths, associated with locally released rock-buffered fluids based on vein isotopic compositions (Figure 8). White symbols denote veins likely formed during their exhumation path. Circles and squares represent data obtained from quartz-calcite oxygen isotope and clumped isotope thermometry, respectively.

reached their maximum burial depths, except for post-mélange veins with $\delta^{18}\text{O} \leq 0\text{‰}$ (Figure 8), likely forming during the exhumation path as discussed earlier (white circles in Figure 9). Some veins record temperatures higher than the maximum burial temperature of the host rocks (Figures 7 and 8), implying a connection to the flow of hotter fluids. This aligns with findings from previous studies, correlating such occurrences with fluid flows along the shear zones (Deweever et al., 2013; Hansberry et al., 2015; Kondo et al., 2005) or up-dip fluid flow (Sadofsky & Bebout, 2004; Vrolijk et al., 1988). These events occur within short timeframes or along permeable horizons, such as plate boundary décollements or out-of-sequence thrust, facilitating focused fluid migration (e.g., Carson & Sreaton, 1998; Moore, 1989). However, the interior of subducted sediments within seismogenic depths generally exhibits low porosity and permeability (e.g., Moore et al., 2007; Saffer & Tobin, 2011), limiting long-distance fluid flow. Locally released fluids from dehydration reactions become the primary source (Raimbourg et al., 2015; Yamaguchi et al., 2012). Therefore, we interpret that most veins we analyzed formed along the subduction path, capturing in situ temperature conditions and isotopic signatures of locally released fluids from surrounding host rocks.

It is important to note that while we anticipate several mélangé units covered by our study to have experienced peak temperatures exceeding 250°C (Table 1 and Figure 1), the absence of available peak temperature records from the literature in the proximity to our sampling locations results in limited data points within the range of 250–350°C (Figure 9). The farthest distance between nearby maximum temperature records and our sample localities could be ~3 km away. Given this distance, the host rock peak temperature can vary by tens of degrees Celsius (e.g., Rajič, Raimbourg, Famin, et al., 2023; Sakaguchi, 1999). Therefore, we suggest that future analyses incorporate host rock peak temperature measurements alongside vein temperature determinations for a more comprehensive analysis.

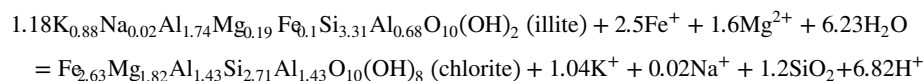
Another complexity arises when interpreting temperatures obtained from clumped isotope thermometry. The apparent equilibrium blocking temperature for calcite is 150–200°C based on models (Henkes et al., 2014; Stolper & Eiler, 2015). If the ambient temperature of the country rocks exceeds this range, there is a potential for the reordering of C–O bonds. For vein temperature potentially related to hotter fluids (dark gray diamonds in Figure 9), recording temperatures higher than the apparent blocking temperature may indicate isotopic re-equilibrium, not reflecting the thermal conditions of the hot fluids (i.e., the actual formation temperatures of vein calcite). The fluids might migrate to colder country rocks, being quenched by their lower temperatures. Eventually, the host rocks would also exhume to colder temperatures. Isotopic re-equilibrium might have occurred until the host rocks reached the apparent blocking temperature, and the recorded temperatures may represent conditions between vein-forming and ambient temperatures. Similar scenarios may be applicable to other temperature records obtained from clumped isotope thermometry (light gray diamonds in Figure 9). Alternately, given that these temperature values closely align with 150–200°C, they may reflect the temperatures at which vein calcite formed without re-equilibrium.

Despite the complexities, it remains evident that most veins preserve temperature records within the range of 100–250°C, coupled with isotopic signatures indicative of rock-buffered fluids. Dehydration reactions, including smectite-illite conversion in the mudstone matrix of tectonic mélanges and the saponite-chlorite transition in altered oceanic crust, have been suggested as sources producing fluids with these isotopic compositions (Raimbourg et al., 2015; Yamaguchi et al., 2012). These reactions align with the proposed major fluid sources near the seismogenic zone at active convergent margins (e.g., Kameda et al., 2011; Kastner et al., 1991; Saffer et al., 2008). Importantly, the smectite-illite transformation also releases silica (e.g., Perry & Hower, 1972; Powers, 1967) from the mudstone matrix, offering a possible silica source for quartz precipitation as veins. For example, in the metapelites of the Kodiak accretionary complex, the following reaction has been observed (Rajič, Raimbourg, Lerouge, et al., 2023):



The temperature range for vein formation we identify correlates well with the operating temperatures of these reactions. The smectite-illite transition can occur within the range of 65–210°C (e.g., Chamley, 1989; Jennings & Thompson, 1986), and the saponite-chlorite transformation takes place within the range of 150–250°C (Kameda et al., 2011; Merriman & Frey, 1999).

At 250–350°C, hydration reactions, primarily chlorite crystallization, become dominant instead. This is supported by studies on mélangé units of the Shimanto belt and Kodiak accretionary complex with paleotemperature records corresponding to the range, where an increase in chlorite content in the mélangé matrix is observed (Rajič, Raimbourg, Lerouge, et al., 2023; Ramirez et al., 2021). Rajič, Raimbourg, Lerouge, et al. (2023) suggest chlorite mainly formed as rims along the contact between veins and matrix through the following reaction:



For the transformation of illite to chlorite, they suggest additional Fe and Mg derived locally are required. These elements are found to be lost in scaly fabrics of mudstone matrix (Chen, Smye, Fisher, et al., 2024; Ramirez et al., 2021), which can serve as a source. Additional H₂O is also required to compensate the greater amount of water in chlorite. The reaction likely consumes H₂O of pore fluid, evidenced by the increase in salinity of FI trapped in mélanges with higher chlorite contents (Rajič, Raimbourg, Lerouge, et al., 2023). Based on these metamorphic reactions, we interpret that the observed temperature regime of 100–250°C, favorable for vein formation, likely correlates with a fluid-saturated condition. Above the temperature threshold, dominated hydration reactions may result in a fluid-undersaturated regime, which is less favorable for vein formation (Figure 9).

5.3. Implication for Subduction Zone Seismogenesis

Mass transfer, sometimes referred to specifically as pressure solution and quartz cementation, is recognized as a potential mechanism influencing seismic behavior along the plate interface (e.g., D. M. Fisher et al., 2021; Giuntoli & Viola, 2021; Moore & Saffer, 2001; Williams & Fagereng, 2022). The mechanism plays a significant role in modulating the mechanical and hydraulic properties of subduction fault zones. The precipitation of redistributed materials, forming mineral veins within cracks of subducted sediments, promotes consolidation. Cemented rocks with low porosity are often characterized as velocity-weakening (Collettini et al., 2019; Lockner & Byerlee, 1986; Tesei et al., 2014), which enhances the likelihood of instability nucleation (Marone, 1998; Scholz, 1998). Crack sealing reduces porosity and permeability, potentially leads to fluid pressure accumulation. The rise in fluid pressure can cause a decrease in effective normal stress, promoting the tendency toward stable slip based on rate- and state- friction laws (Scholz, 1998). However, laboratory experiments also suggest that fluid overpressure may promote slip instability by modulating other rate- and state- friction parameters (Scuderi & Collettini, 2016). Hooker and Fisher (2021) develop a numerical model integrating mechanical and hydraulic effects of mass transfer on fault slip. They predict a process where mass transfer promotes cementations, resulting in the build-up of fluid pressure, while coseismic slip ruptures the seal, leading to a drop in fluid pressure.

Our observations indicate the prevalence of fluid-driven mass transfer within temperature range of 100–250°C, as evidenced by the temperature of vein formation. During interseismic periods, prominent crack-sealing processes may promote consolidation of subducted sediments, leading to their tendency toward velocity-weakening behavior. Vein precipitation coupled with fluid released from hydrous minerals (as outlined in Section 5.2) likely results in an accumulation of fluid pressure within this temperature/depth range along the plate interface. This exerts contrasting effects on fault stability—promoting stable slip by decreasing effective normal stress, while potentially inducing instabilities through alterations in other rate- and state- friction parameters. In the 250–350°C range, subduction fault zones are anticipated to become fluid-unsaturated due to hydration reactions such as chlorite crystallization. Combined with reduced crack-sealing, fluid pressure is expected to decrease, increasing effective normal stress but exerting less control on rate- and state-friction parameters. However, the quantification of the diminished fluid budget resulting from these reactions and consideration of the viscous response of the matrix to pore fluid reduction remains crucial. Our study highlights a potential for mechanical and hydraulic variations within the thermal conditions of 100–350°C along the plate boundary, arising from fluid-mineral interactions. A quantitative constraint on the degree of fluid pressure change would be invaluable for future laboratory experiments aimed at exploring the impact of fluid pressure on subduction zone fault stability.

6. Conclusions

We apply quartz-calcite oxygen isotope thermometry and carbonate clumped isotope thermometry to analyze the isotopic compositions and temperature records of quartz and calcite grains in veins from a suite of tectonic mélange units in the Cretaceous Shimanto belt and Kodiak accretionary complex. The C-isotopic signatures of calcite suggest its origin from both organic matter and sedimentary carbonates. The O-isotopic signatures indicate that the vein-forming fluid sources include meteoric water, seawater, and rock-buffering fluids. The differing $\delta^{18}\text{O}$ values observed in quartz from the Cretaceous Shimanto belt and Kodiak accretionary complex may be indicative of their distinct paleogeographic locations. The consistent temperature records within the range of 100–250°C observed in the veins are likely attributed to the availability of fluid sources at corresponding depths along the plate interface. The prevalence of mass transfer in the temperature range, combined with clay dehydration, may contribute to a high fluid pressure regime. As temperatures rise to 250–350°C, reduced vein precipitation coupled with hydration reactions may mark a potential shift in hydrogeology and mechanics within subduction fault zones. This transition is characterized by an increase in effective normal stress and a reduced influence of fluid pressure on rate- and state-friction parameters.

Data Availability Statement

The SIMS and clumped isotope analysis data presented in this paper are available at Zenodo via <https://doi.org/10.5281/zenodo.10461479> with open access.

Acknowledgments

This study received funding from the National Science Foundation (NSF) through two awards: EAR-1524530 and EAR-2214324 from the Tectonics Program, both awarded to D. Fisher. T.-W. Chen received support through the 2020 and 2022 GSA Graduate Student Research Grant. We would like to thank M. Liu, A. Hertwig, E. Bell, N. Matsuda, and K. McKeegan at the UCLA SIMS lab for the support of SIMS data collection, M. Ingalls for the technical support in clumped isotope data collection, and H. Leapaldt for the help with the method description. Finally, we express sincere gratitude to two anonymous reviewers for their constructive feedback, which significantly improved this manuscript. We also extend our appreciation to the editor, W. Behr, for overseeing the review process.

References

- Anderson, N. T., Kelson, J. R., Kele, S., Daëron, M., Bonifacie, M., Horita, J., et al. (2021). A unified clumped isotope thermometer calibration (0.5–1,100°C) using carbonate-based standardization. *Geophysical Research Letters*, *48*(7), e2020GL092069. <https://doi.org/10.1029/2020GL092069>
- Barker, C. E. (1988). Geothermics of petroleum systems: Implications of the stabilization of kerogen thermal maturation after a geologically brief heating duration at peak temperature. In *Petroleum systems of the United States* (Vol. 1870, pp. 26–29). US Geological Survey Bulletin.
- Bernasconi, S. M., Daëron, M., Bergmann, K. D., Bonifacie, M., Meckler, A. N., Affek, H. P., et al. (2021). InterCarb: A community effort to improve interlaboratory standardization of the carbonate clumped isotope thermometer using carbonate standards. *Geochemistry, Geophysics, Geosystems*, *22*(5), e2020GC009588. <https://doi.org/10.1029/2020GC009588>
- Bostick, N. H., Cashman, S. M., McCulloh, T. H., & Waddell, C. T. (1978). Gradients of vitrinite reflectance and present temperature in the Los Angeles and Ventura basins, California. In D. F. Oltz (Ed.), *Low temperature Metamorphism of Kerogen and clay minerals* (pp. 65–96). Society of Economic Paleontologists and Mineralogists, Pacific Section Symposium in Geochemistry.
- Brand, W. A., Assonov, S. S., & Coplen, T. B. (2010). Correction for the ¹⁷O interference in δ (¹³C) measurements when analyzing CO₂ with stable isotope mass spectrometry (IUPAC Technical Report). *Pure and Applied Chemistry*, *82*(8), 1719–1733. <https://doi.org/10.1351/PAC-REP-09-01-05>
- Brantley, S. L., Fisher, D. M., Clark, M. B., Myers, G., & Deines, P. (1997). Segregation veins: Evidence for the deformation and dewatering of a low-grade metapelite. In M. B. Holness (Ed.), *Deformation-enhanced fluid transport in the earth's crust and mantle* (pp. 266–287). Chapman and Hall.
- Byrne, T. (1984). Early deformation in mélange terranes of the Ghost Rocks Formation, Kodiak islands, Alaska. *Melanges: Their Nature, Origin, and Significance*, *198*, 21–52. <https://doi.org/10.1130/SPE198-p21>
- Carson, B., & Sreaton, E. J. (1998). Fluid flow in accretionary prisms: Evidence for focused, time-variable discharge. *Reviews of Geophysics*, *36*(3), 329–351. <https://doi.org/10.1029/97RG03633>
- Cerchiari, A., Remitti, F., Mittempergher, S., Festa, A., Lugli, F., & Cipriani, A. (2020). Cyclical variations of fluid sources and stress state in a shallow megathrust-zone mélange. *Journal of the Geological Society*, *177*(3), 647–659. <https://doi.org/10.1144/jgs2019-072>
- Chamley, H. (1989). *Clay sedimentology*. Springer.
- Chen, T.-W., Smye, A., Lloyd, M., Fisher, D., & Hashimoto, Y. (2024). Temperatures of vein formation associated with plate interface deformation constrained by oxygen and clumped isotope thermometry [Dataset]. *Zenodo*. <https://doi.org/10.5281/zenodo.10461479>
- Chen, T.-W., Smye, A. J., Fisher, D. M., Hashimoto, Y., Raimbourg, H., & Famin, V. (2024). Quantifying interseismic volume strain from chemical mass-balance analysis in tectonic mélanges. *Geochemistry, Geophysics, Geosystems*, *25*(1), e2023GC011241. <https://doi.org/10.1029/2023GC011241>
- Colletini, C., Tesi, T., Scuderi, M. M., Carpenter, B. M., & Viti, C. (2019). Beyond Byerlee friction, weak faults and implications for slip behavior. *Earth and Planetary Science Letters*, *519*, 245–263. <https://doi.org/10.1016/j.epsl.2019.05.011>
- Daëron, M., Blamart, D., Peral, M., & Affek, H. P. (2016). Absolute isotopic abundance ratios and the accuracy of Δ⁴⁷ measurements. *Chemical Geology*, *442*, 83–96. <https://doi.org/10.1016/j.chemgeo.2016.08.014>
- Dansgaard, W. (1964). Stable isotopes in precipitation. *Tellus*, *16*(4), 436–468. <https://doi.org/10.3402/tellusa.v16i4.8993>
- Deweever, B., Swennen, R., & Breesch, L. (2013). Fluid flow compartmentalization in the Sicilian fold and thrust belt: Implications for the regional aqueous fluid flow and oil migration history. *Tectonophysics*, *591*, 194–209. <https://doi.org/10.1016/j.tecto.2011.08.009>
- Eberl, D. D., Srodon, J., Lee, M., Nadeau, P. H., & Northrop, H. R. (1987). Sericite from the Silverton Caldera, Colorado; correlation among structure, composition, origin, and particle thickness. *American Mineralogist*, *72*(9–10), 914–934.
- England, P. C., & Smye, A. J. (2023). Metamorphism and deformation on subduction interfaces: 1. Physical framework. *Geochemistry, Geophysics, Geosystems*, *24*(1), e2022GC010644. <https://doi.org/10.1029/2022GC010644>
- Fisher, D., & Byrne, T. (1987). Structural evolution of underthrust sediments, Kodiak Islands, Alaska. *Tectonics*, *6*(6), 775–793. <https://doi.org/10.1029/TC006i006p00775>
- Fisher, D. M., Hooker, J. N., Smye, A. J., & Chen, T. W. (2021). Insights from the geological record of deformation along the subduction interface at depths of seismogenesis. *Geosphere*, *17*(6), 1686–1703. <https://doi.org/10.1130/GES02389.1>
- Fisher, D. M., Smye, A. J., Marone, C., Van Keken, P. E., & Yamaguchi, A. (2019). Kinetic models for healing of the subduction interface based on observations of ancient accretionary complexes. *Geochemistry, Geophysics, Geosystems*, *20*(7), 3431–3449. <https://doi.org/10.1029/2019GC008256>
- Frey, M. (1987). Very low-grade metamorphism of clastic sedimentary rocks. In M. Frey (Ed.), *Low temperature metamorphism* (pp. 9–58). Chapman and Hall.
- Gallen, S. F. (2008). *An investigation of the magnetic fabrics and the paleomagnetism of the Ghost Rocks Formation, Kodiak islands, Alaska. (Doctoral dissertation)*. Western Washington University. Retrieved from <https://cedar.wvu.edu/wwuet/11>
- Ghosh, P., Adkins, J., Affek, H., Balta, B., Guo, W., Schauble, E. A., et al. (2006). ¹³C–¹⁸O bonds in carbonate minerals: A new kind of paleothermometer. *Geochimica et Cosmochimica Acta*, *70*(6), 1439–1456. <https://doi.org/10.1016/j.gca.2005.11.014>
- Giuntoli, F., & Viola, G. (2021). Cyclic brittle-ductile oscillations recorded in exhumed high-pressure continental units: A record of deep episodic tremor and slow slip events in the northern Apennines. *Geochemistry, Geophysics, Geosystems*, *22*(9), e2021GC009805. <https://doi.org/10.1029/2021GC009805>
- Hansberry, R. L., Collins, A. S., King, R. C., Morley, C. K., Gize, A. P., Warren, J., et al. (2015). Syn-deformation temperature and fossil fluid pathways along an exhumed detachment zone, Khao Khwang fold-thrust belt, Thailand. *Tectonophysics*, *655*, 73–87. <https://doi.org/10.1016/j.tecto.2015.05.012>
- Hara, H., & Kimura, K. (2008). Metamorphic and cooling history of the Shimanto accretionary complex, Kyushu, Southwest Japan: Implications for the timing of out-of-sequence thrusting. *Island Arc*, *17*(4), 546–559. <https://doi.org/10.1111/j.1440-1738.2008.00636.x>
- Hashimoto, Y., Eida, M., Kirikawa, T., Iida, R., Takagi, M., Furuya, N., et al. (2012). Large amount of fluid migration around shallow seismogenic depth preserved in tectonic mélange: Yokonami mélange, the Cretaceous Shimanto Belt, Kochi, Southwest Japan. *Island Arc*, *21*(1), 53–64. <https://doi.org/10.1111/j.1440-1738.2011.00806.x>
- Hashimoto, Y., Enjoji, M., Sakaguchi, A., & Kimura, G. (2002). PT conditions of cataclastic deformation associated with underplating: An example from the Cretaceous Shimanto complex, Kii Peninsula, SW Japan. *Earth Planets and Space*, *54*(11), 1133–1138. <https://doi.org/10.1186/bf03353314>
- Hashimoto, Y., Enjoji, M., Sakaguchi, A., & Kimura, G. (2003). In situ pressure–temperature conditions of a tectonic mélange: Constraints from fluid inclusion analysis of syn-mélange veins. *Island Arc*, *12*(4), 357–365. <https://doi.org/10.1046/j.1440-1738.2003.00405.x>

- Henkes, G. A., Passey, B. H., Grossman, E. L., Shenton, B. J., Pérez-Huerta, A., & Yancey, T. E. (2014). Temperature limits for preservation of primary calcite clumped isotope paleotemperatures. *Geochimica et Cosmochimica Acta*, *139*, 362–382. <https://doi.org/10.1016/j.gca.2014.04.040>
- Hooker, J. N., & Fisher, D. M. (2021). How cementation and fluid flow influence slip behavior at the subduction interface. *Geology*, *49*(9), 1074–1078. <https://doi.org/10.1130/G48741.1>
- Hower, J., Eslinger, E. V., Hower, M. E., & Perry, E. A. (1976). Mechanism of burial metamorphism of argillaceous sediment: 1. Mineralogical and chemical evidence. *Geological Society of America Bulletin*, *87*(5), 725–737. [https://doi.org/10.1130/0016-7606\(1976\)87<725:MOBMOA>2.0.CO;2](https://doi.org/10.1130/0016-7606(1976)87<725:MOBMOA>2.0.CO;2)
- Hyndman, R. D., Yamano, M., & Oleskevich, D. A. (1997). The seismogenic zone of subduction thrust faults. *Island Arc*, *6*(3), 244–260. <https://doi.org/10.1111/j.1440-1738.1997.tb00175.x>
- Ikesawa, E., Kimura, G., Sato, K., Ikehara-Ohmori, K., Kitamura, Y., Yamaguchi, A., et al. (2005). Tectonic incorporation of the upper part of oceanic crust to overriding plate of a convergent margin: An example from the Cretaceous–early Tertiary Mugi Mélange, the Shimanto Belt, Japan. *Tectonophysics*, *401*(3–4), 217–230. <https://doi.org/10.1016/j.tecto.2005.01.005>
- Jennings, S., & Thompson, G. R. (1986). Diagenesis of Plio-Pleistocene sediments of the Colorado River delta, southern California. *Journal of Sedimentary Research*, *56*(1), 89–98. <https://doi.org/10.1306/212F8891-2B24-11D7-8648000102C1865D>
- Kameda, J., Yamaguchi, A., Saito, S., Sakuma, H., Kawamura, K., & Kimura, G. (2011). A new source of water in seismogenic subduction zones. *Geophysical Research Letters*, *38*(22), L22306. <https://doi.org/10.1029/2011GL048883>
- Kastner, M., Elderfield, H., & Martin, J. B. (1991). Fluids in convergent margins: What do we know about their composition, origin, role in diagenesis and importance for oceanic chemical fluxes? *Philosophical Transactions of the Royal Society of London. Series A: Physical and Engineering Sciences*, *335*(1638), 243–259. <https://doi.org/10.1098/rsta.1991.0045>
- Kelly, J. L., Fu, B., Kita, N. T., & Valley, J. W. (2007). Optically continuous silcrete quartz cements of the St. Peter Sandstone: High precision oxygen isotope analysis by ion microprobe. *Geochimica et Cosmochimica Acta*, *71*(15), 3812–3832. <https://doi.org/10.1016/j.gca.2007.05.014>
- Kiminami, K., & Ohno, Y. (1999). *Vitrinite reflectance and contact metamorphism on argillites by basaltic rocks in an accretionary complex: An example from the Late Cretaceous Makimine Formation, Kyushu* (Vol. 52, pp. 243–253). Memoir of the Geological Society Japan. (in Japanese with English Abstract).
- Kimura, G., Yamaguchi, A., Hojo, M., Kitamura, Y., Kameda, J., Ujiie, K., et al. (2012). Tectonic mélange as fault rock of subduction plate boundary. *Tectonophysics*, *568*, 25–38. <https://doi.org/10.1016/j.tecto.2011.08.025>
- Kisch, H. J. (1987). Correlation between indicators of very low-grade metamorphism. In M. Frey (Ed.), *Low temperature metamorphism* (pp. 227–300). Chapman and Hall.
- Kitamura, Y., & Kimura, G. (2012). Dynamic role of tectonic mélange during interseismic process of plate boundary mega earthquakes. *Tectonophysics*, *568*, 39–52. <https://doi.org/10.1016/j.tecto.2011.07.008>
- Kitamura, Y., Sato, K., Ikesawa, E., Ikehara-Ohmori, K., Kimura, G., Kondo, H., et al. (2005). Mélange and its seismogenic roof décollement: A plate boundary fault rock in the subduction zone—An example from the Shimanto belt, Japan. *Tectonics*, *24*(5), TC5012. <https://doi.org/10.1029/2004TC001635>
- Kondo, H., Kimura, G., Masago, H., Ohmori-Ikehara, K., Kitamura, Y., Ikesawa, E., et al. (2005). Deformation and fluid flow of a major out-of-sequence thrust located at seismogenic depth in an accretionary complex: Nobeoka Thrust in the Shimanto Belt, Kyushu, Japan. *Tectonics*, *24*(6), 1–16. <https://doi.org/10.1029/2004TC001655>
- Kreutzberger, M. E., & Peacor, D. R. (1988). Behavior of illite and chlorite during pressure solution of shaly limestone of the Kalkberg Formation, Catskill, New York. *Journal of Structural Geology*, *10*(8), 803–811. [https://doi.org/10.1016/0191-8141\(88\)90096-X](https://doi.org/10.1016/0191-8141(88)90096-X)
- Leapaldt, H. (2022). *Seasonal lacustrine carbonate early diagenesis driven by microbial metabolisms in Green Lake, New York* (Master dissertation). Pennsylvania State University. Retrieved from <https://etda.libraries.psu.edu/catalog/19578hcl5089>
- Li, J., Shillington, D. J., Bécel, A., Nedimović, M. R., Webb, S. C., Saffer, D. M., et al. (2015). Down-dip variations in seismic reflection character: Implications for fault structure and seismogenic behavior in the Alaska subduction zone. *Journal of Geophysical Research: Solid Earth*, *120*(11), 7883–7904. <https://doi.org/10.1002/2015JB012338>
- Lockner, D. A., & Byerlee, J. D. (1986). *Laboratory measurements of velocity-dependent frictional strength*. Department of the Interior, US Geological Survey.
- Logan, J. M., & Rauenzahn, K. A. (1987). Frictional dependence of gouge mixtures of quartz and montmorillonite on velocity, composition and fabric. *Tectonophysics*, *144*(1–3), 87–108. [https://doi.org/10.1016/0040-1951\(87\)90010-2](https://doi.org/10.1016/0040-1951(87)90010-2)
- Marin, J., Chaussidon, M., & Robert, F. (2010). Microscale oxygen isotope variations in 1.9 Ga Gunflint cherts: Assessments of diagenesis effects and implications for oceanic paleotemperature reconstructions. *Geochimica et Cosmochimica Acta*, *74*(1), 116–130. <https://doi.org/10.1016/j.gca.2009.09.016>
- Marone, C. (1998). Laboratory-derived friction laws and their application to seismic faulting. *Annual Review of Earth and Planetary Sciences*, *26*(1), 643–696. <https://doi.org/10.1146/annurev.earth.26.1.643>
- Masuda, H., Kusakabe, M., & Sakai, H. (1992). Hydrogen and oxygen isotope ratios of shales and characteristics of formation waters in sedimentary complexes accreted at different times, Kinki district, southwest Japan. *Geochimica et Cosmochimica Acta*, *56*(9), 3505–3511. [https://doi.org/10.1016/0016-7037\(92\)90394-X](https://doi.org/10.1016/0016-7037(92)90394-X)
- Matsumura, M., Hashimoto, Y., Kimura, G., Ohmori-Ikehara, K., Enjohji, M., & Ikesawa, E. (2003). Depth of oceanic-crust underplating in a subduction zone: Inferences from fluid-inclusion analyses of crack-seal veins. *Geology*, *31*(11), 1005–1008. <https://doi.org/10.1130/G19885.1>
- Meneghini, F., Marroni, M., Moore, J. C., Pandolfi, L., & Rowe, C. D. (2009). The processes of underthrusting and underplating in the geologic record: Structural diversity between the Franciscan complex (California), the Kodiak complex (Alaska) and the internal Ligurian units (Italy). *Geological Journal*, *44*(2), 126–152. <https://doi.org/10.1002/gj.1144>
- Merriman, R., & Frey, M. (1999). Patterns of very low-grade metamorphism in metapelitic rocks. In M. Frey & R. Merriman (Eds.), *Low-grademetamorphism* (pp. 61–107). Blackwell Science.
- Moore, J. C. (1989). Tectonics and hydrogeology of accretionary prisms: Role of the décollement zone. *Journal of Structural Geology*, *11*(1–2), 95–106. [https://doi.org/10.1016/0191-8141\(89\)90037-0](https://doi.org/10.1016/0191-8141(89)90037-0)
- Moore, J. C., Byrne, T., Plumley, P. W., Reid, M., Gibbons, H., & Coe, R. S. (1983). Paleogene evolution of the Kodiak Islands, Alaska: Consequences of ridge-trench interaction in a more southerly latitude. *Tectonics*, *2*(3), 265–293. <https://doi.org/10.1029/TC002i003p00265>
- Moore, J. C., Rowe, C., & Meneghini, F. (2007). How accretionary prisms elucidate seismogenesis in subduction zones. In T. H. Dixon & J. C. Moore (Eds.), *The seismogenic zone of subduction thrust faults* (pp. 288–315). Columbia University Press. <https://doi.org/10.7312/dix013866-010>

- Moore, J. C., & Saffer, D. (2001). Updip limit of the seismogenic zone beneath the accretionary prism of southwest Japan: An effect of diagenetic to low-grade metamorphic processes and increasing effective stress. *Geology*, 29(2), 183–186. [https://doi.org/10.1130/0091-7613\(2001\)029<0183:ULOTSZ>2.0.CO;2](https://doi.org/10.1130/0091-7613(2001)029<0183:ULOTSZ>2.0.CO;2)
- Mukoyoshi, H., Hirono, T., Hara, H., Sekine, K., Tsuchiya, N., Sakaguchi, A., & Soh, W. (2009). Style of fluid flow and deformation in and around an ancient out-of-sequence thrust: An example from the Nobeoka Tectonic Line in the Shimanto accretionary complex, Southwest Japan. *Island Arc*, 18(2), 333–351. <https://doi.org/10.1111/j.1440-1738.2009.00670.x>
- Mukoyoshi, H., Sakaguchi, A., Otsuki, K., Hirono, T., & Soh, W. (2006). Co-seismic frictional melting along an out-of-sequence thrust in the Shimanto accretionary complex. Implications on the tsunamigenic potential of splay faults in modern subduction zones. *Earth and Planetary Science Letters*, 245(1–2), 330–343. <https://doi.org/10.1016/j.epsl.2006.02.039>
- Myers, G., & Vrolijk, P. J. (1986). Fluid evolution associated with the accretion of the Kodiak Formation, Kodiak island, Alaska. *EOS, Transactions, American Geophysical Union*, 67, 1219.
- Newman, A. V., Schwartz, S. Y., Gonzalez, V., DeShon, H. R., Protti, J. M., & Dorman, L. M. (2002). Along-strike variability in the seismogenic zone below Nicoya Peninsula, Costa Rica. *Geophysical Research Letters*, 29(20), 38–1. <https://doi.org/10.1029/2002GL015409>
- Ogunyomi, O., Hesse, R., & Héroux, Y. (1980). Pre-orogenic and synorogenic diagenesis and anchimetamorphism in Lower Paleozoic continental margin sequences of the northern Appalachians in and around Québec City, Canada. *Bulletin of Canadian Petroleum Geology*, 28(4), 559–577. <https://doi.org/10.35767/gscpgbull.28.4.559>
- Oleskevich, D. A., Hyndman, R. D., & Wang, K. (1999). The updip and downdip limits to great subduction earthquakes: Thermal and structural models of Cascadia, south Alaska, SW Japan, and Chile. *Journal of Geophysical Research*, 104(B7), 14965–14991. <https://doi.org/10.1029/1999JB900060>
- O'Neil, J. R., Clayton, R. N., & Mayeda, T. K. (1969). Oxygen isotope fractionation in divalent metal carbonates. *The Journal of Chemical Physics*, 51(12), 5547–5558. <https://doi.org/10.1063/1.1671982>
- Peacock, S. M., & Hyndman, R. D. (1999). Hydrous minerals in the mantle wedge and the maximum depth of subduction thrust earthquakes. *Geophysical Research Letters*, 26(16), 2517–2520. <https://doi.org/10.1029/1999GL900558>
- Perry, E. A., Jr., & Hower, J. (1972). Late-stage dehydration in deeply buried pelitic sediments. *AAPG Bulletin*, 56(10), 2013–2021. <https://doi.org/10.1306/819A41A8-16C5-11D7-8645000102C1865D>
- Powers, M. C. (1967). Fluid-release mechanisms in compacting marine mudrocks and their importance in oil exploration. *AAPG Bulletin*, 51(7), 1240–1254. <https://doi.org/10.1306/5d25c137-16c1-11d7-8645000102c1865d>
- Raimbourg, H., Famin, V., Palazzin, G., Yamaguchi, A., & Augier, R. (2017). Tertiary evolution of the Shimanto belt (Japan): A large-scale collision in early Miocene. *Tectonics*, 36(7), 1317–1337. <https://doi.org/10.1002/2017TC004529>
- Raimbourg, H., Famin, V., Palazzin, G., Yamaguchi, A., Augier, R., Kitamura, Y., & Sakaguchi, A. (2019). Distributed deformation along the subduction plate interface: The role of tectonic mélanges. *Lithos*, 334, 69–87. <https://doi.org/10.1016/j.lithos.2019.01.033>
- Raimbourg, H., Rajič, K., Moris-Muttoni, B., Famin, V., Palazzin, G., Fisher, D., et al. (2021). Quartz vein geochemistry records deformation processes in convergent zones. *Geochemistry, Geophysics, Geosystems*, 22(4), e2020GC009201. <https://doi.org/10.1029/2020GC009201>
- Raimbourg, H., Vacelet, M., Ramboz, C., Famin, V., Augier, R., Palazzin, G., et al. (2015). Fluid circulation in the depths of accretionary prisms: An example of the Shimanto belt, Kyushu, Japan. *Tectonophysics*, 655, 161–176. <https://doi.org/10.1016/j.tecto.2015.05.023>
- Rajič, K., Raimbourg, H., Famin, V., Moris-Muttoni, B., Fisher, D. M., Morell, K. D., & Canizarés, A. (2023). Exhuming an accretionary prism: A case study of the Kodiak accretionary complex, Alaska, USA. *Tectonics*, 42(10), e2023TC007754. <https://doi.org/10.1029/2023TC007754>
- Rajič, K., Raimbourg, H., Lerouge, C., Famin, V., Dubacq, B., Canizarés, A., et al. (2023). Metamorphic reactions and their implication for the fluid budget in metapelites at seismogenic depths in subduction zones. *Tectonophysics*, 229844, 229844. <https://doi.org/10.1016/j.tecto.2023.229844>
- Ramirez, G., Smye, A., Fisher, D. M., Hashimoto, Y., & Yamaguchi, A. (2021). Constraints on element mobility during deformation within the seismogenic zone, Shimanto belt, Japan. *Geochemistry, Geophysics, Geosystems*, 22(8), e2020GC009594. <https://doi.org/10.1029/2020GC009594>
- Sadofsky, S. J., & Bebout, G. E. (2001). Paleohydrogeology at 5- to 50-kilometer depths of accretionary prisms: The Franciscan Complex, California. *Geophysical Research Letters*, 28(12), 2309–2312. <https://doi.org/10.1029/2000GL008533>
- Sadofsky, S. J., & Bebout, G. E. (2004). Field and isotopic evidence for fluid mobility in the Franciscan complex: Forearc paleohydrogeology to depths of 30 kilometers. *International Geology Review*, 46(12), 1053–1088. <https://doi.org/10.2747/0020-6814.46.12.1053>
- Saffer, D. M., & Marone, C. (2003). Comparison of smectite- and illite-rich gouge frictional properties: Application to the updip limit of the seismogenic zone along subduction megathrusts. *Earth and Planetary Science Letters*, 215(1–2), 219–235. [https://doi.org/10.1016/S0012-821X\(03\)00424-2](https://doi.org/10.1016/S0012-821X(03)00424-2)
- Saffer, D. M., & Tobin, H. J. (2011). Hydrogeology and mechanics of subduction zone forearcs: Fluid flow and pore pressure. *Annual Review of Earth and Planetary Sciences*, 39(1), 157–186. <https://doi.org/10.1146/annurev-earth-040610-133408>
- Saffer, D. M., Underwood, M. B., & McKiernan, A. W. (2008). Evaluation of factors controlling smectite transformation and fluid production in subduction zones: Application to the Nankai Trough. *Island Arc*, 17(2), 208–230. <https://doi.org/10.1111/j.1440-1738.2008.00614.x>
- Sakaguchi, A. (1996). High paleogeothermal gradient with ridge subduction beneath the Cretaceous Shimanto accretionary prism, southwest Japan. *Geology*, 24(9), 795–798. [https://doi.org/10.1130/0091-7613\(1996\)024<0795:HPGWRS>2.3.CO;2](https://doi.org/10.1130/0091-7613(1996)024<0795:HPGWRS>2.3.CO;2)
- Sakaguchi, A. (1999). Thermal structure and paleo-heat flow in the Shimanto accretionary prism, Southwest Japan. *Island Arc*, 8(3), 359–372. <https://doi.org/10.1046/j.1440-1738.1999.00246.x>
- Sample, J. C., & Moore, J. C. (1987). Structural style and kinematics of an underplated slate belt, Kodiak and adjacent islands, Alaska. *Geological Society of America Bulletin*, 99(1), 7–20. [https://doi.org/10.1130/0016-7606\(1987\)99<7:SSAKOA>2.0.CO;2](https://doi.org/10.1130/0016-7606(1987)99<7:SSAKOA>2.0.CO;2)
- Scholz, C. H. (1998). *The mechanics of earthquakes and faulting*. Cambridge University Press.
- Scholz, C. H. (1998). Earthquakes and friction laws. *Nature*, 391(6662), 37–42. <https://doi.org/10.1038/34097>
- Scuderi, M. M., & Collettini, C. (2016). The role of fluid pressure in induced vs. triggered seismicity: Insights from rock deformation experiments on carbonates. *Scientific Reports*, 6(1), 24852. <https://doi.org/10.1038/srep24852>
- Seno, T. (2005). Variation of downdip limit of the seismogenic zone near the Japanese islands: Implications for the serpentinization mechanism of the forearc mantle wedge. *Earth and Planetary Science Letters*, 231(3–4), 249–262. <https://doi.org/10.1016/j.epsl.2004.12.027>
- Sharp, Z. D., & Kirschner, D. L. (1994). Quartz-calcite oxygen isotope thermometry: A calibration based on natural isotopic variations. *Geochimica et Cosmochimica Acta*, 58(20), 4491–4501. [https://doi.org/10.1016/0016-7037\(94\)90350-6](https://doi.org/10.1016/0016-7037(94)90350-6)
- Smeraglia, L., Aldega, L., Bernasconi, S. M., Billi, A., Boschi, C., Caracausi, A., et al. (2020). The role of trapped fluids during the development and deformation of a carbonate/shale intra-wedge tectonic mélange (Mt. Massico, Southern Apennines, Italy). *Journal of Structural Geology*, 138, 104086. <https://doi.org/10.1016/j.jsg.2020.104086>

- Stolper, D. A., & Eiler, J. M. (2015). The kinetics of solid-state isotope-exchange reactions for clumped isotopes: A study of inorganic calcites and apatites from natural and experimental samples. *American Journal of Science*, *315*(5), 363–411. <https://doi.org/10.2475/05.2015.01>
- Sweeney, J. J., & Burnham, A. K. (1990). Evaluation of a simple model of vitrinite reflectance based on chemical kinetics. *AAPG Bulletin*, *74*(10), 1559–1570. <https://doi.org/10.1306/OC9B251F-1710-11D7-8645000102C1865D>
- Taira, A. (1980). The geology of the Shimanto belt in Kochi prefecture, Shikoku, Japan. In *Geology and paleontology of the Shimanto belt* (pp. 319–389).
- Taira, A., Katto, J., Tashiro, M., Okamura, M., & Kodama, K. (1988). The Shimanto belt in Shikoku, Japan—evolution of cretaceous to Miocene accretionary prism. *Modern Geology*, *12*, 5–46.
- Taira, A., Okada, H., Whitaker, J. H., & Smith, A. J. (1982). The Shimanto belt of Japan: Cretaceous-lower Miocene active-margin sedimentation. *Geological Society, London, Special Publications*, *10*(1), 5–26. <https://doi.org/10.1144/gsl.sp.1982.010.01.01>
- Tesei, T., Collettini, C., Barchi, M. R., Carpenter, B. M., & Di Stefano, G. (2014). Heterogeneous strength and fault zone complexity of carbonate-bearing thrusts with possible implications for seismicity. *Earth and Planetary Science Letters*, *408*, 307–318. <https://doi.org/10.1016/j.epsl.2014.10.021>
- Toriumi, M., & Teruya, J. (1988). Tectono-metamorphism of the Shimanto belt. *Modern Geology*, *12*(1–4), 303–324.
- Ujiiie, K., Saishu, H., Fagereng, Å., Nishiyama, N., Otsubo, M., Masuyama, H., & Kagi, H. (2018). An explanation of episodic tremor and slow slip constrained by crack-seal veins and viscous shear in subduction mélange. *Geophysical Research Letters*, *45*(11), 5371–5379. <https://doi.org/10.1029/2018GL078374>
- Underwood, M. B., Laughland, M. M., & Kang, S. M. (1993). A comparison among organic and inorganic indicators of diagenesis and low-temperature metamorphism, Tertiary Shimanto belt, Shikoku, Japan. In M. B. Underwood (Ed.), *Thermal evolution of the tertiary Shimanto belt, southwest Japan: An example of ridge-trench interaction*. Geological Society of America special paper (Vol. 273, pp. 45–61). Geological Society of America. <https://doi.org/10.1130/spe273-p45>
- Vrolijk, P. (1990). On the mechanical role of smectite in subduction zones. *Geology*, *18*(8), 703–707. [https://doi.org/10.1130/0091-7613\(1990\)018<0703:OTMROS>2.3.CO;2](https://doi.org/10.1130/0091-7613(1990)018<0703:OTMROS>2.3.CO;2)
- Vrolijk, P., Myers, G., & Moore, J. C. (1988). Warm fluid migration along tectonic melanges in the Kodiak accretionary complex, Alaska. *Journal of Geophysical Research*, *93*(B9), 10313–10324. <https://doi.org/10.1029/JB093iB09p10313>
- Williams, R. T., & Fagereng, Å. (2022). The role of quartz cementation in the seismic cycle: A critical review. *Reviews of Geophysics*, *60*(1), e2021RG000768. <https://doi.org/10.1029/2021RG000768>
- Yamaguchi, A., Ishikawa, T., Kato, Y., Nozaki, T., Meneghini, F., Rowe, C. D., et al. (2014). Fluid-rock interaction recorded in black fault rocks in the Kodiak accretionary complex, Alaska. *Earth Planets and Space*, *66*, 1–7. <https://doi.org/10.1186/1880-5981-66-58>
- Yamaguchi, A., Ujiiie, K., Nakai, S. I., & Kimura, G. (2012). Sources and physicochemical characteristics of fluids along a subduction-zone megathrust: A geochemical approach using syn-tectonic mineral veins in the Mugi mélange, Shimanto accretionary complex. *Geochemistry, Geophysics, Geosystems*, *13*(7), Q0AD24. <https://doi.org/10.1029/2012GC004137>
- Yang, C., & Hesse, R. (1991). Clay minerals as indicators of diagenetic and anchimetamorphic grade in an overthrust belt, external domain of southern Canadian Appalachians. *Clay Minerals*, *26*(2), 211–231. <https://doi.org/10.1180/claymin.1991.026.2.06>